A single neuron in *C. elegans* orchestrates multiple motor outputs through parallel modes of transmission

Yung-Chi Huang[1], Jinyue Luo[1], Wenjia Huang[2], Casey M. Baker[1], Matthew A. Gomes[1], Bohan Meng[1], Alexandra B. Byrne[2], Steven W. Flavell[1,*]

[1]Picower Institute for Learning & Memory, Department of Brain & Cognitive Sciences, Massachusetts Institute of Technology, Cambridge, MA, USA
[2]Department of Neurobiology, UMass Chan Medical School, Worcester, MA, USA
[*]Corresponding Author: flavell@mit.edu

SUMMARY

Animals generate a wide range of highly coordinated motor outputs, which allows them to execute purposeful behaviors. Individual neurons in the circuits that generate behaviors have a remarkable capacity for flexibility, as they exhibit multiple axonal projections, transmitter systems, and modes of neural activity. How these multi-functional properties of neurons enable the generation of adaptive behaviors remains unknown. Here we show that the HSN neuron in *C. elegans* evokes multiple motor programs over different timescales to enable a suite of behavioral changes during egg-laying. Using HSN activity perturbations and in vivo calcium imaging, we show that HSN acutely increases egg-laying and locomotion while also biasing the animals towards low-speed dwelling behavior over minutes. The acute effects of HSN on egg-laying and high-speed locomotion are mediated by separate sets of HSN transmitters and different HSN axonal compartments. The long-lasting effects on dwelling are mediated in part by HSN release of serotonin, which is taken up and re-released by NSM, another serotonergic neuron class that directly evokes dwelling. Our results show how the multi-functional properties of a single neuron allow it to induce a coordinated suite of behaviors and also reveal that neurons can borrow serotonin from one another to control behavior.

INTRODUCTION

Individual neurons are the basic units of computation in the brain. While some neuron classes have straightforward functional roles, many others exhibit complex multi-functional roles. First, neurons can exhibit multiple modes of dynamics. For example, in the stomatogastric ganglion of crustaceans, individual neuron classes can be co-active with multiple oscillatory networks, each with their own rhythm, and influence activity in each of these networks[1,2]. Neuron classes whose activities are associated with multiple motor programs have also been identified in worms, flies, and mice[3–6]. Second, neurons can co-release multiple transmitters[7]. For example, in *C. elegans*, RIM neurons control escape responses via release of glutamate, acetylcholine, tyramine, and neuropeptides[8–10]. In mammals, midbrain dopamine neurons co-release GABA to modulate basal ganglia circuits[11]. Third, neurons can contain multiple electrotonically isolated compartments[12,13]. In vivo studies that relate these multi-functional properties of neurons to animal behavior remain limited.

The roundworm *C. elegans* provides a tractable system for dissecting the functional properties of individual neurons in the context of behavior. There are 302 neurons in the *C. elegans* nervous system and the connectivity among these neurons is known[14–16]. *C. elegans* exhibit a well-characterized set of motor programs[17] that are extensively coordinated with one another[18–21] and can be flexibly generated depending on the context[22]. These include locomotion, egg-laying, head and body posture, defecation, and feeding. Mechanisms that underlie the coordination of these motor programs are still mostly unknown.

The egg-laying behavior of *C. elegans* is controlled by a neural circuit that innervates the vulval muscles whose contraction causes egg-laying[23]. A key neuron in the egg-laying circuit is HSN, which synapses onto VC neurons and vulval muscles and has a command-like role in controlling egg-laying. HSN also extends a neurite to the nerve ring in the head where it synapses with neurons in other circuits (Fig. 1A). However, the function of this projection to the nerve ring is not yet understood. HSN releases acetylcholine, serotonin, and several neuropeptides[23,24] and receives diverse modulatory inputs[25,26]. In freely-moving animals, HSN exhibits calcium peaks that are sometimes accompanied by egg-laying[19,27]; its release of serotonin and the NLP-3 neuropeptide is required for egg-laying[28]. HSN's effects on egg-laying appear to be coordinated with changes in locomotion. Egg-laying is correlated with high-speed locomotion[18,20], which depends on the AVF neuron and dopamine signaling[18,20]. Somewhat paradoxically, ablation of HSN or reduced serotonin production in HSN impairs low-speed dwelling states, which are stable periods of slow locomotion on food[29,30]. The cellular mechanisms that explain the diverse impacts of HSN on these distinct behaviors are still unclear.

Here, we examine the cellular mechanisms that allow HSN to exert multiple influences on behavior. We show that HSN plays a causal role in driving egg-laying and high-speed locomotion during egg-laying while also eliciting low-speed dwelling over minutes-long timescales. HSN increases egg-laying and acute locomotion via different transmitters and distinct subcellular compartments. In addition, serotonin released from HSN acts over minutes to induce low-speed dwelling. This effect is due in part to serotonin being taken up and re-released by the serotonergic neuron NSM in the head that directly evokes dwelling. Our results reveal how a single neuron can influence a broad suite of behaviors over multiple timescales and show that neurons can 'borrow' serotonin from one another to control behavior.

RESULTS

HSN neurons induce acute egg-laying and speeding, as well as long-term slowing

To examine the causal effect of HSN activity on behavior (Fig. 1A), we performed gain- and loss-of-function perturbations to HSN. To activate HSN, we generated a strain with HSN-specific expression of the blue light-sensitive opsin CoChR[31]. There were no promoters known to drive expression uniquely in HSN, so we developed an intersectional approach for cell-specific expression based on the *cat-4* and *egl-6* promoters (Fig. 1B; Fig. S1A shows specificity; we refer to this strain as HSN::CoChR). We first examined the effects of activating HSN::CoChR with blue light in animals that were dwelling on a food source. HSN activation evoked an immediate

increase in egg-laying, as previously reported[25] (Fig. 1C). In addition, we observed an immediate increase in forward locomotion speed (Fig. 1C; Fig. S1B). Since HSN activation had not been shown to induce speeding before, we performed additional controls to ensure that this effect was specifically due to HSN activation. We examined the effect of activating HSN::CoChR in *egl-1(gf)* mutants, where HSN dies from programmed cell death[32]. This abolished the light-induced increase in egg-laying and locomotion speed, indicating that both effects are due to HSN activation (Fig. 1D). We also examined whether the increase in locomotion speed was a consequence of egg-laying or, alternatively, a parallel output. To test this, we activated HSN in animals sterilized with FUDR. In these animals, there were no eggs, but HSN stimulation still increased locomotion speed (Fig. 1E). Taken together, these experiments indicate that HSN activity acutely increases egg-laying and forward locomotion and that the effect on locomotion is separable from HSN's effect on egg-laying.

We also examined the effects of HSN activation under conditions where animals were travelling at high speed due to recent transfer to a low-density food plate. HSN activation still increased locomotion during light stimulation, but this was followed by an acute reduction in locomotion that lasted for minutes (Fig. 1F). This slowing effect remained intact in animals sterilized with FUDR, suggesting that it was not dependent on egg-laying (Fig. S1C). Together with the above results, this suggest that HSN activation promotes acute egg-laying and high-speed locomotion, followed by a reduction in locomotion speed.

We next examined the impact of endogenous HSN activity on locomotion. For these experiments, we utilized *egl-1(gf)* mutants in which HSN is specifically killed. *egl-1(gf)* mutants are known to exhibit reduced egg-laying[32]. We examined whether the eggs that are laid in the mutant are accompanied by increased locomotion, as is the case in wild-type. To do so, we recorded egg-laying and locomotion simultaneously and examined animal speed surrounding egg-laying. Consistent with previous data[20], wild-type animals displayed increased forward movement before and during egg-laying, but this was disrupted in *egl-1(gf)* mutants (Fig. 1G). This indicates that HSN is required for speeding prior to egg-laying and matches our finding that HSN activation increases speed and egg-laying. *egl-1(gf)* animals actually displayed a speed reduction prior to egg-laying, which could be due to other components of the egg-laying circuit that remain intact in *egl-1(gf)*. We also examined dwelling behavior in *egl-1(gf)* mutants using an assay that quantifies animal exploration across a bacterial food lawn. As described previously, *egl-1(gf)* mutants displayed reduced dwelling behavior (or, equivalently, increased roaming; Fig. 1H)[30]. This indicates that HSN is necessary for proper dwelling and matches our findings that HSN activation can increase dwelling for minutes after optogenetic stimulation. Taken together, these data indicate that HSN is required for increased locomotion speed surrounding egg-laying events and low-speed dwelling on bacterial food.

HSN activity is correlated with egg-laying and increased locomotion

The above experiments suggest that HSN activity induces acute egg-laying and speeding, as well as long-term slowing. We next examined how endogenous HSN activity was coupled to

these behaviors. We generated a strain expressing GCaMP5A and mScarlett in HSN and performed ratiometric imaging as animals freely moved at low speed on bacterial food lawns. HSN activity was organized into discrete calcium peaks that commonly occurred in bursts (Fig. 2A), as previously described[19,27,33,34]. Egg-laying was invariably coupled to HSN calcium peaks (Fig. 2B and S2A). However, there were many calcium peaks that were not accompanied by egg-laying. We also examined animal speed surrounding HSN calcium peaks and found that the peaks were on average time-locked to transient increases in speed (Fig. 2C and S2B). This effect was just as robust when excluding the HSN peaks associated with egg-laying (Fig. S2C). This suggests that HSN calcium peaks are often accompanied by egg-laying and increased animal speed.

HSN calcium peaks often occur in bursts[19,27]. Based on an analysis of inter-peak intervals, HSN peaks within one minute of one another appeared likely to be part of the same burst (Fig. S2D). We examined whether HSN peaks differed in their correlation with behavior depending on whether they occurred earlier or later in bursts. HSN calcium peaks that were associated with egg-laying most frequently occurred later in bursts, shortly after several other peaks (Fig. 2D). In contrast, HSN calcium peaks were most strongly correlated with locomotion speed when there were fewer previous HSN peaks (Fig. 2E; see also Fig. S2E). Thus, when several HSN calcium peaks occur in close succession, earlier peaks are associated with increased locomotion and later peaks are associated with egg-laying. These data provide evidence that endogenous HSN activity is acutely correlated with speeding and egg-laying.

To examine the intrinsic coupling of HSN activity to motor networks, we also examined HSN activity in immobilized animals. During immobilization, the *C. elegans* nervous system exhibits fictive locomotion dynamics where neurons that encode forward and reverse movement switch between high and low activity states[35–37]. RIB is one of the forward-active neurons and its bi-stable activity reports the fictive locomotion state of the network. Therefore, we recorded HSN and RIB simultaneously. HSN calcium peaks were significantly more likely to occur when RIB activity was high (Fig. S2F-G), suggesting that HSN activity is coupled to the forward locomotion network even in the absence of actual movement.

HSN increases locomotion speed through its neuropeptidergic outputs

We next sought to determine which HSN transmitter(s) mediate these behavioral effects. To determine the transmitters that underlie HSN-induced speeding, we performed optogenetic HSN stimulation in mutant backgrounds lacking specific HSN transmitters. HSN evokes egg-laying via serotonin and NLP-3 neuropeptides[28]. However, animals lacking serotonin (*tph-1* mutants) or both serotonin and NLP-3 still displayed increased speed upon HSN::CoChR activation (Fig. 3A-B). HSN also releases acetylcholine[38], so we examined its impact on HSN-induced speeding. Animals fully deficient in acetylcholine release are uncoordinated[39]. Therefore, we engineered a conditional knockout allele of *unc-17*, which encodes the vesicular acetylcholine transporter (VAChT)[40] required for acetylcholine release (Fig. 3C; see Methods for validation). However, animals with an HSN-specific deletion of *unc-17* still displayed robust

HSN-induced speeding (Fig. 3D). This suggests that serotonin, NLP-3, and HSN-produced acetylcholine are not essential for HSN-induced speeding.

Several neuropeptides are expressed in HSN, according to previous gene expression studies[24,41,42]. Thus, we next asked whether HSN neuropeptide production is required for HSN-induced speeding. We examined HSN-induced speeding in animals with a null mutation in *egl-21*, which encodes a carboxypeptidase required for the production of many neuropeptides[43]. HSN-induced speeding was abolished in these mutants (Fig. 3E). However, *egl-21* is expressed very broadly, so it was unclear whether this effect was due to loss of neuropeptide production in HSN or other neurons. Therefore, we examined HSN-induced speeding in a strain harboring an HSN-specific deletion of *egl-21* (Fig. 3F). We used *egl-6*::nCre to inactivate *egl-21* in HSN (along with ~5 other neurons that express *egl-6*)[26] and found that this abolished HSN-induced speeding (Fig. 3G; Fig. S3A shows no effect on baseline velocity off food). This suggests that HSN neuropeptide production is required for HSN-induced speeding.

We attempted to determine which HSN neuropeptide(s) mediate HSN-induced speeding. We obtained a panel of 12 mutants lacking neuropeptides reported to be expressed in HSN[24,41,42]. We examined speeding surrounding native egg-laying events in each of these single mutants. Of these, *flp-26* and *flp-28* impacted animal speed surrounding egg-laying (Fig. S3B-D; other mutants had no effect). We also crossed neuropeptide mutants into HSN::CoChR and found that loss of *flp-2* and *flp-26* partially attenuated HSN-induced speeding (Fig. 3H-J). This suggests that *flp-2*, *flp-26*, and *flp-28* may be involved in egg-laying- or HSN-induced speeding. *flp-2* is known to impact locomotion[44], but *flp-26* and *flp-28* have not been closely examined. We made compound mutants lacking multiple neuropeptides and found that both HSN-induced speeding and the native coupling of speeding to egg-laying were attenuated in double mutants lacking *flp-2* and *flp-28* (Fig. 3K-L). HSN-specific expression of *flp-2* and *flp-28* in the double mutant restored normal HSN-induced speeding (Fig. 3M). Taken together, these experiments suggest that HSN acutely increases locomotion via its release of neuropeptides, including *flp-2* and *flp-28*.

HSN serotonin promotes slow locomotion and NSM-induced slowing

We next examined which HSN transmitter(s) drive the decrease in locomotion speed over longer time scales. Here, we analyzed baseline dwelling behavior and HSN-stimulated slowing (see Fig. 1F). We first examined serotonin and NLP-3, the HSN transmitters that control egg-laying[28]. We found that *tph-1* mutants (lacking serotonin) displayed decreased baseline dwelling (Fig. 4A) and a reduction in HSN-stimulated slowing, particularly several minutes after stimulation (Fig. 4B and D). Animals lacking *nlp-3* had normal baseline dwelling (Fig. 4A) and normal HSN-stimulated slowing (Fig. 4C-D; see also Fig. S4A). We previously showed that cell-specific *tph-1* deletion in HSN also causes a deficit in dwelling[30]. Here, we found that HSN-specific *tph-1* expression partially rescued the *tph-1* mutant deficit in dwelling, suggesting that HSN-produced serotonin is sufficient to drive dwelling (Fig. 4E). Thus, multiple lines of evidence suggest that HSN serotonin promotes dwelling behavior.

We characterized the timescale over which HSN influences low-speed dwelling on food. As shown above, HSN activation induces low-speed dwelling with a short latency and these effects last for minutes. To determine the timescale over which native HSN activity controls dwelling, we examined how long it takes for chemogenetic HSN silencing (with a histamine-gated chloride channel, HisCl[45]) to alter dwelling on food. We first used egg-laying assays to characterize how quickly HSN is inactivated after HSN::HisCl animals are transferred to histamine-containing plates. Egg-laying was inhibited within 5min of transfer, suggesting that HSN is silenced within minutes after histamine exposure (Fig. S4B). We then determined the time course of the effect of HSN silencing on low-speed dwelling behavior. Animals were recorded right after being transferred onto histamine-containing plates. HSN-silenced animals showed significantly higher speed only after 30-40min of histamine exposure (Fig. 4F). This suggests that HSN needs to be inactivated for tens of minutes for there to be an increase in speed, revealing a long-lasting effect.

Given this slow time scale, we hypothesized that HSN-released serotonin influences dwelling by contributing to the tonic pool of serotonin. In addition to directly interacting with downstream serotonin receptors, extracellular serotonin might be taken up by other serotonergic neurons via MOD-5[46,47], the serotonin transporter (SERT), and re-released to influence behavior (Fig. 4G and S4G). The serotonergic neuron NSM in particular expresses high levels of *mod-5*.[46,47] NSM is activated by feeding; its activity is correlated with dwelling and NSM activation drives dwelling via serotonin release[6,48–50] (Fig. 4G). It can produce its own serotonin, but it was unclear whether NSM serotonin can also be supplied by other neurons. Thus, we next examined whether HSN-produced serotonin could be taken up and re-released by NSM to influence dwelling.

A key prediction of this hypothesis is that NSM's ability to induce slow locomotion via serotonin release should depend on HSN serotonin production. To test this, we used an assay where we optogenetically activated NSM. Consistent with previous work[50], we found that optogenetic NSM activation evoked slowing in a *tph-1*-dependent manner, indicating that NSM serotonin drives slowing (Fig. S4C). We next examined whether animals that only have *tph-1* expressed in HSN displayed a rescue in NSM-induced slowing. Indeed, restoring HSN serotonin production via HSN::*tph-1* expression partially rescued the ability of optogenetic NSM stimulation to induce slowing (Fig. 4H). This suggests that HSN serotonin production can partially rescue NSM-induced slowing.

We next performed a complementary experiment where we tested whether the loss of HSN (via *egl-1* mutation) in a wild-type background impairs the ability of NSM to induce slow locomotion. Indeed, there was a significant reduction in NSM-induced slowing in *egl-1(gf)* mutants (Fig. 4I). This suggests that HSN is required for normal NSM-induced slowing.

These results are consistent with two possible interpretations. First, HSN serotonin might be taken up by NSM via MOD-5/SERT, such that altering HSN serotonin production alters NSM's ability to evoke slow locomotion via serotonin re-release. Alternatively, HSN serotonin may be required downstream of NSM activation for slowing. To distinguish between these possibilities, we tested whether HSN could still influence NSM-stimulated slowing in a mutant

background where *mod-5/*SERT was deleted. If the first interpretation is correct, there should be no additional effect of HSN ablation on NSM-stimulated slowing if *mod-5* is already deleted, since the *mod-5* mutation would already prevent extracellular serotonin from being taken up by NSM. Alternatively, if NSM-stimulated slowing requires a downstream function of HSN, then HSN ablation should still affect NSM-induced slowing even when *mod-5* is absent. Thus, we compared the effects of optogenetic NSM stimulation on locomotion in *mod-5* mutants versus *mod-5;egl-1(gf)* double mutants. We performed this experiment using a range of different light intensities to ensure that we were examining NSM-induced slowing under conditions where slowing was non-saturating (Fig. 4J; see Fig. S4D-F for multiple light intensities). This was necessary because the loss of *mod-5* leads to hyper-enhanced slowing, since released serotonin cannot be rapidly cleared by MOD-5/SERT[47,51]. At all light levels tested, there was no difference between the two strains (Fig. 4I-J). This indicates that HSN only impacts NSM-induced slowing when *mod-5*/SERT-dependent serotonin re-uptake is intact. Taken together, this set of experiments suggests that HSN serotonin is taken up and re-released by NSM to evoke slow locomotion.

The distinct behavioral functions of HSN map onto different subcellular compartments

HSN causally influences behavior in at least three ways: (1) it drives acute egg-laying through serotonin and NLP-3 release; (2) it drives acute speeding through release of neuropeptides; and (3) it drives dwelling over longer time scales via serotonin release. We next asked how these distinct functions of HSN map onto its unique anatomy. The HSN soma is in the mid-body, posterior to the vulva (Fig. 5A), and its neurite projects anteriorly towards the head[15]. In the region where it passes over the vulva, HSN extends short branches where it synapses with vulval muscles and VC neurons (the 'vulval presynaptic region'). The main HSN axon then enters the ventral cord, projects anteriorly, and enters the nerve ring in the head, where it makes synapses with other neurons.

How does HSN activity propagate across the neuron? Previous work showed that HSN calcium peaks in the soma occur normally even when the HSN axon is severed before reaching the vulval presynaptic region[33]. This suggests that the HSN activity peaks can originate in the soma. To determine whether HSN soma calcium peaks are accompanied by calcium peaks along the entire axon, we performed calcium imaging of the whole HSN neuron in immobilized animals and examined signals in the soma, vulval presynaptic region, and distal axon near the nerve ring (Fig. 5B). HSN calcium peaks in each compartment were accompanied by calcium peaks in the other compartments (Fig. 5C), suggesting that calcium peaks are rapidly propagated across the entire neuron.

Next, we mapped out sites of transmitter release in HSN, focusing on serotonin. *cat-1* encodes the *C. elegans* vesicular monoamine transporter (VMAT) that loads serotonin into synaptic vesicles. Its subcellular localization can be used as an indicator of serotonin-containing vesicle release sites[52]. Because *cat-1* is broadly expressed, we generated a strain to visualize endogenous CAT-1 localization in individual neurons, like HSN. We engineered a strain with

three tandem repeats of the split-GFP fragment GFP11 inserted before the native *cat-1* stop codon, creating an in-frame fusion protein (Fig. 5D). We then expressed the other split-GFP fragment GFP1-10 under the *egl-6* promoter that drives expression in HSN, but no other *cat-1*-expressing neurons. When GFP1-10 interacts with CAT-1-3xGFP11 in HSN it reconstitutes a functional GFP fluorophore. Reconstituted CAT-1::GFP in HSN displayed punctate localization, suggestive of presynaptic release sites, matching previous non-cell-specific CAT-1 immunostaining[52]. HSN CAT-1::GFP puncta were brightest in the vulval presynaptic region, with much weaker fluorescence in the head and no expression along the neurite (Fig. 5E; Fig. S5A). EM studies indicated that HSN synapses in the mid-body are larger than those in the head, which may be related to the difference we observed here[15]. This suggests that HSN primarily releases serotonin in the vulval presynaptic region.

We also tested which behavioral functions of HSN require its axonal projection to the nerve ring. To do so, we examined animals where we axotomized the HSNL/R neurites just anterior to the vulval presynaptic region (Fig. 5F; Fig. S5B shows exact cut site). This leaves the HSN soma connected to the vulval presynaptic region but not to the remainder of the neurite that projects into the nerve ring. Egg-laying rates were unaffected by laser axotomy at this position (Fig. 5G), consistent with the notion that the HSN vulval presynaptic region controls egg-laying. However, egg-laying in the axotomized animals displayed much weaker coupling to increased locomotion speed (Fig. 5H; laser controls in Fig. S5C). This suggests that HSN signal propagation to the head is required for proper speeding during egg-laying. In contrast, the baseline speed of animals on food was not significantly affected by HSN axotomy (Fig. 5I). Thus, disrupting the HSN axonal projection to the nerve ring does not bias the animals towards roaming, even though HSN cell ablation or HSN silencing does (Fig. 5I; and above). Together, these experiments suggest that HSN axonal projections to the head are required for acute speeding during egg-laying but not baseline egg-laying or baseline on-food locomotion.

Sensory control of egg-laying requires humoral release of neuropeptides by sensory neurons

The above results provide information about how the functional outputs of HSN map onto the different anatomical and molecular features of this neuron. We also wanted to examine how sensory inputs are transmitted to HSN, given its unique anatomy and function. Egg-laying behavior is impacted by many aspects of the sensory environment, including food availability, aversive cues, and more[53–56]. Here, we focused on the effects of osmolarity, as it has been shown that a mild upshift in osmolarity (< 1 Osm) triggers reduced egg-laying[33,57] and reduced HSN activity[33], suggesting that this may be a good system for studying sensory control over HSN activity and behavior.

To examine how high osmolarity inhibits HSN and egg-laying, we used an assay where animals were transferred to a high osmolarity plate for one hour and the number of eggs laid was counted (Fig. 6A). Osmolarity was increased beyond the normal 150 mOsm level by addition of sorbitol. This revealed a dose-dependent effect where higher levels of osmolarity in the plate

inhibited egg-laying (Fig. 6B; baseline egg-laying rates in Fig. S6A). To determine the sensory mechanisms that link osmolarity to egg-laying, we examined behavioral responses of animals lacking either *tax-2* or *ocr-2*, which encode ion channels required for sensory transduction in different sensory neurons[58]. While *ocr-2* mutants still responded to the osmotic stimulus, *tax-2* mutants had an attenuated response at 300 mOsm (Fig. 6B-C). Higher concentrations still inhibited egg-laying in *tax-2*, suggesting that additional mechanisms may inhibit egg-laying under those conditions. We observed the same behavioral phenotype in animals lacking *tax-4*, which encodes ion channel subunits that function together with TAX-2 (Fig. 6C)[58].

We asked whether these mild 300 mOsm conditions that reduced egg-laying were sufficient to impact HSN activity using GCaMP imaging in moving animals. Indeed, HSN calcium peak frequency was significantly reduced in the animals on 300 mOsm agar, compared to standard 150 mOsm conditions (Fig. S6B).

To map out which exact sensory neurons are required for osmolarity-induced egg-laying inhibition, we performed two sets of experiments. First, we examined behavioral responses in a panel of transgenic and mutant strains with specific sensory neurons ablated. Second, we examined behavioral responses in animals that had *tax-4* rescued in different sensory neurons to recover their sensory transduction. We examined the effects of cell ablation for >10 sensory cell types and only observed an attenuated behavioral response in animals with the sensory neuron BAG ablated (Fig. 6D; Fig. S6C). We examined the effects of restoring *tax-4* expression in seven neuron classes and observed the most robust rescue when *tax-4* was rescued in BAG (Fig. 6E; Fig. S6D). Consistent with the *tax-2* mutant results above, BAG ablation did not prevent the reduction in egg-laying caused by higher osmolarity levels (Fig. S6E). This suggest that sensory transduction in BAG sensory neurons is important for osmolarity-induced inhibition of egg-laying.

BAG senses gases through its ciliated sensory ending[59,60]. To test whether BAG responds to changes in osmolarity, we performed BAG GCaMP imaging in freely-moving animals as they moved from a 150 mOsm agar environment to a 300 mOsm environment (generated by fusing agar; see Methods). Indeed, BAG calcium levels increased as animals moved to the higher osmolarity environment (Fig. 6F). This suggests that BAG either directly senses osmolarity upshifts or receives inputs from other osmo-sensitive cells.

We attempted to characterize the BAG signal that is required for osmolarity-induced inhibition of egg-laying behavior. BAG is the main source of FLP-17 and one of the sources of FLP-10[61]. Both of these neuropeptides inhibit HSN, so we examined osmolarity-induced behavioral responses in mutants lacking these neuropeptides[26]. *flp-17* mutants, as well as animals lacking the FLP-17 receptor *egl-6*, showed an attenuated egg-laying response to osmolarity upshift, matching BAG-ablated animals (Fig. 6G; Fig. S6F). This suggests that FLP-17/EGL-6 signaling is important for osmolarity-induced egg-laying inhibition. Related to this, we also found that HSN axotomy (in the position described above) did not attenuate the effects of osmolarity on egg-laying (Fig. 6H). This suggests that a humoral signal is relayed from sensory neurons to HSN to inhibit egg-laying, rather than local synaptic signaling in the head. Overall, these results suggest that increased osmolarity activates a BAG-FLP-17 signal to inhibit egg-

laying. Given the known role of FLP-17/EGL-6 signaling in inhibiting HSN and our observation that exposure to 300 mOsm conditions activates BAG and inhibits HSN, this effect may be mediated by HSN inhibition. In addition, we have not ruled out the presence of other osmolarity-induced changes that may impact egg-laying in parallel.

DISCUSSION

Animals coordinate many distinct motor outputs as they execute purposeful behaviors. Here, we show how specific multi-functional properties of the HSN neuron endow it with the ability to orchestrate a suite of behavioral changes. HSN promotes an acute increase in egg-laying and locomotion, followed by low-speed dwelling behavior. The acute effects on egg-laying and speeding are mediated by distinct sets of HSN transmitters and different subcellular compartments. The longer lasting effect on dwelling is mediated by HSN release of serotonin, which is taken up and re-released by serotonergic NSM neurons that directly evoke dwelling. Our results illustrate how cellular morphology, multiple transmitter systems, and non-canonical modes of transmission like neurotransmitter "borrowing" endow a single neuron with the ability to orchestrate multiple features of a behavioral program.

While the role of HSN in egg-laying is well-established[23,56], we used optical tools to reveal additional behavioral functions of HSN. We found that HSN releases multiple neuropeptides to acutely increase locomotion speed prior to egg-laying. Our axotomy data suggest that the speed-evoking effect of HSN requires its axon in the head. Given that the locomotion circuit is located in the head and that HSN calcium peaks are reliably transmitted along the HSN axon, these peptides may be well positioned to exert fast, direct action on locomotion circuits during HSN calcium peaks. We also found that HSN serotonin can induce dwelling behavior that lasts for minutes after HSN activity ends. Interestingly, HSN-released serotonin is taken up and re-released by NSM in the head, which directly drives dwelling. After serotonin is released, it can be absorbed by different cell types via the serotonin transporter, MOD-5/SERT[46,62,63]. In *C. elegans,* the neurons NSM, AIM, and RIH neurons have been shown to absorb endogenous and exogenous serotonin in a *mod-5*-dependent manner [46,47,64]. However, it has remained unclear whether this absorption is for serotonin turnover/degradation or, alternatively, whether this serotonin is re-released to impact behavior. Our work here provides evidence that serotonin can be transferred between serotonergic neurons and re-released to control behavior. Recent expression studies suggest that similar mechanisms could potentially occur for GABA as well[65]. This mechanism of neurotransmitter "borrowing" may be functionally important. NSM is activated by feeding and its release of serotonin evokes dwelling[49,66]. Our results here suggest that serotonin levels in NSM are influenced by HSN activity. This might allow HSN activity to have a priming-like effect, where its recent activity could increase NSM serotonin levels so that subsequent food-driven NSM activation could lead to more robust slowing. Future studies could make use of fluorescent serotonin sensors[67,68] to define the spatiotemporal dynamics of this extra-synaptic serotonin more precisely.

The behavioral coordination that HSN facilitates during egg-laying could be evolutionarily adaptive. One possible reason that animals may increase locomotion during egg-laying may be to depolarize muscle cells adjacent to vulval muscles, facilitating egg-laying. In addition, high-speed movement during egg-laying may allow animals to distribute their eggs rather than depositing them all in one location. Coupled with HSN's ability to bias animals towards dwelling, this could allow animals to distribute their eggs within a high-quality environment and dwell in the overall vicinity as well. *C. elegans* egg-laying is impacted by many aspects of the sensory environment – food, aversive cues, and more[23]. We found that high osmolarity, an aversive stimulus, signals through a humoral factor to inhibit egg-laying. Together, HSN's sensory inputs and its outputs that couple egg-laying to locomotion may allow animals to distribute their eggs across favorable sensory environments.

ACKNOWLEDGMENTS

We thank Mark Alkema, Cori Bargmann, and members of the Flavell lab for critical reading of the manuscript; Cori Bargmann for guidance during mosSCI strain generation; the Caenorhabditis Genetics Center (supported by P40 OD010440), Bob Horvitz, Piali Sengupta, and Cori Bargmann for strains; and Yun Zhang and Nuria Flames for sharing plasmids and DNA sequences. A.B.B. acknowledges funding from NIH (NS124338). Y-C.H. was supported by a Picower Fellowship. S.W.F. acknowledges funding from NIH (GM135413); NSF (Award #1845663); McKnight Foundation; Alfred P. Sloan Foundation; The Picower Institute for Learning and Memory; and The JPB Foundation.

AUTHOR CONTRIBUTIONS

Conceptualization, Y-C.H. and S.W.F. Methodology, Y-C.H., J.L., W.H., C.M.B., M.A.G., A.B.B., and S.W.F. Software, Y-C.H., C.M.B., and S.W.F. Formal analysis, Y-C.H. and S.W.F. Investigation, Y-C.H., J.L., W.H., C.M.B., M.A.G., B.M., A.B.B., and S.W.F. Writing – Original Draft, Y-C.H. and S.W.F Writing – Review & Editing, Y-C.H. and S.W.F. Funding Acquisition, A.B.B. and S.W.F.

DECLARATION OF INTERESTS

The authors have no competing interests to declare.

FIGURE LEGENDS

Figure 1. The HSN neuron evokes egg-laying, acute speeding, and long-term slowing

(A) Cartoon showing HSN neuron (red) in *C. elegans*. Pharyngeal and vulval muscles are light gray; eggs are dark gray.

(B) Intersectional promoter strategy for HSN-specific expression of CoChR. An inverted CoChR-sl2-GFP cassette is expressed under the *cat-4* promoter. The *egl-6* promoter drives expression of Cre recombinase, which acts on the lox sites to invert CoChR-sl2-GFP.

(C) Behavioral responses to HSN::CoChR activation, shown as averages of velocity (top) or egg-laying (bottom) aligned to optogenetic stimuli. Blue boxes indicate the light illumination period. For velocity, statistics examined whether the change in velocity during lights-on was different between the two groups (see Methods). For egg-laying, statistics examined whether the egg-laying rate during lights-on was different between the two groups. Because egg-laying events are transient, the mean for the egg-laying rate over time is a jagged line. n = 37 animals (470 stimulation events) for +ATR and 12 animals (120 stimulation events) for -ATR. ****p<0.0001, Mann-Whitney U test.

(D) HSN::CoChR activation in *egl-1(n487gf)* mutants. n = 10 animals (144 stimulation events) for *egl-1*. WT data is same as (C). ****p<0.0001, Mann-Whitney U test, as in (C).

(E) HSN::CoChR activation in animals treated with FUDR. n = 20 animals (250 stimulation events) for FUDR-treated animals. WT data is same as (C). ****p<0.0001, Mann-Whitney U test, as in (C).

(F) Effect of HSN::CoChR activation on speed in animals travelling at high baseline speeds, shown as average speed aligned to optogenetic stimuli. n = 100-112 animals. Statistics examined whether the change in speed (minute before stimulation versus minute after stimulation) was different between groups. ****p<0.0001, Mann-Whitney U test.

(G) Change in animal velocity surrounding native, spontaneous egg-laying events. Lines show change in velocity relative to baseline (-5 to -3 min). n = 21 animals for wild-type (518 egg events) and 20 animals for *egl-1* (169 egg events). Statistics examined whether the change in velocity preceding egg-laying was different between groups (see Methods). ****p<0.0001, Mann-Whitney U test.

(H) **Top:** Behavioral assay for exploration. **Bottom:** Exploratory behavior of the indicated genotypes. Dots are individual animals. n = 20 animals for each genotype ***p<0.001, Mann-Whitney U test.

Data are shown as means ± standard error of the mean (SEM).

See also Figure S1.

Figure 2. HSN activity is correlated with egg-laying and locomotion

(A) Example of HSN GCaMP and speed in a freely-moving animal.

(B) Average HSN GCaMP aligned to egg-laying events. n = 16 egg-laying events. **p<0.01, empirical p-value, comparing to shuffle controls in Fig. S2A.

(C) **Left:** Average speed (black) and HSN GCaMP (green) aligned to HSN calcium peaks. **Right:** zoomed-on plot of derivative of HSN GCaMP and speed. n = 104 peaks across 15 animals. **p<0.01, empirical p-value, comparing to shuffle controls in Fig. S2B.

(D) Number of HSN peaks in the minute before HSN peaks that either result in egg-laying or not. Dots are individual peaks. †p=0.0544, Wilcoxon rank-sum test.

(E) Event-triggered averages displayed as in (C), splitting data based on how many HSN calcium peaks occurred before the HSN calcium peak being examined. n = 22-47 peaks per plot. **p<0.01, empirical p-value, determined as in (C).

For (B)-(E), data are shown as mean ± SEM.

See also Figure S2.

Figure 3. HSN evokes acute speeding through its neuropeptidergic outputs

(A-B) HSN::CoChR-induced behavioral changes. Alleles: *tph-1(mg280)* and *nlp-3(n4897)*. n = 7 animals (140 stimulation events) for *tph-1* and 11 animals (180 stimulation events) for *tph-1;nlp-3* animals. WT data is same as Fig. 1C. *p<0.05, ****p<0.0001, Mann-Whitney U test, as in Fig. 1C.

(C) Cartoon of *unc-17*/VAChT conditional knockout allele.

(D) HSN::CoChR activation in floxed *unc-17* animals expressing *pegl-6::Cre*. n = 12 animals (120 stimulation events) for *unc-17* HSN knockout. WT data is same as Fig. 1C. *p<0.05, Mann-Whitney U test, as in Fig. 1C.

(E) HSN::CoChR activation in *egl-21*(*n476)* animals. n = 14 animals (205 stimulation events) for *egl-21*. WT data is same as Fig. 1C. ****p<0.0001, Mann-Whitney U test, as in Fig. 1C.

(F) Cartoon of strain where a single-copy, floxed *egl-21* rescue was introduced into *egl-21(n476)* null animals.

(G) HSN::CoChR activation in HSN-specific *egl-21* knockouts (*egl-21(n476); floxed egl-21 genomic (kySi61);* plus *pegl-6::Cre*). n = 15 animals (150 stimulation events) for *egl-21* strain. WT data is same as Fig. 1C. ****p<0.0001, Mann-Whitney U test, as in Fig. 1C.

(H-K) HSN::CoChR activation in neuropeptide mutants. Alleles: *flp-2(gk1039)*, *flp-28(flv11)*, *flp-26(gk3015)*, and *flp-2(flv15);flp-28(flv11)*. For mutants, n=16-26 animals (160-255 stimulation events). WT data is same as Fig. 1C. *p<0.05, **p<0.01, ***p<0.001, ****p<0.0001, Mann-Whitney U test, as in Fig. 1C, Bonferroni-corrected for single mutants.

(L) Average changes in velocity surrounding native egg-laying events, shown as in Fig. 1G. n = 17 animals for *flp-2; flp-28* (432 egg laying events). WT is the same as in Fig. 1G. *p<0.05, Mann-Whitney U test, determined as in Fig. 1G.

(M) HSN::CoChR-induced behavioral changes. HSN rescue promoter was *Pcat-4prom68*. These datasets are different from those in (K). WT: n = 17 animals (170 stimulation events); *flp-2;flp-28*: n = 22 animals (220 stimulation events); and rescue: n = 10 animals (100 stimulation events). *p<0.05, Mann-Whitney U test, as in Fig. 1C.

Data are shown as means ± SEM.

See also Figure S3.

Figure 4. HSN serotonin promotes slow locomotion and contributes to NSM-induced slowing

(A) Exploratory behavior of indicated genotypes. Alleles: *tph-1(mg280)* and *nlp-3(n4897)*. Dots are individual animals. n = 19–24 animals. ****p<0.0001, Mann-Whitney U test.

(B-C) HSN::CoChR-induced speed changes for indicated genotypes, shown as in Fig. 1F. n = 85-182 animals. Asterisk is based on quantification in (D).

(D) Quantification of data in (B-C), showing speed decrease 1 min or 2-5 min after HSN stimulation (relative to pre-stimulus baseline). *p<0.01, Mann-Whitney U test.

(E) Exploratory behavior of indicated genotypes. Promoters used: *tph-1* (3kb) for all serotonergic neurons; *egl-6* for HSN. Dots are individual animals. n = 11 – 30 animals. ***p<0.01, ****p<0.0001, Mann-Whitney U test.

(F) Average speed over time during HSN chemogenetic silencing. HSN::HisCl is *Pegl-6::HisCl*. **Left:** instantaneous speed. **Right:** same data, binning into 10 min intervals. n = 202-208 animals. *p<0.05, ****p<0.0001. Bonferroni-corrected t-test.

(G) Cartoon illustrating serotonin release and re-uptake by NSM and HSN neurons. HSN does not appear to express *mod-5* (Taylor et al., 2021; Duerr et al., 1999).

(H) Change in animal speed upon NSM::Chrimson stimulation in the indicated genotypes. Animals were starved for 3 hours before the assays. n = 253-351 animals. ****p<0.0001, Mann-Whitney U test examining speed during light illumination.

(I) NSM::Chrimson stimulation in wild-type and *egl-1* animals. n = 85-202 animals. ****p<0.0001, Mann-Whitney U test, as in (H).

(J) NSM::Chrimson stimulation in indicated genotypes. n = 56-209 animals. ****p<0.0001, Mann-Whitney U test**. **Asterisks between panels (I) and (J) indicate a significance difference in the effect of the *egl-1* mutation in an otherwise wild-type background, compared to the effect of *egl-1* in a *mod-5* background, empirical p-value based on computing bootstrap differences.

Data are shown as means ± SEM.

See also Figure S4.

Figure 5. The distinct outputs of HSN map onto different sub-cellular compartments

(A) HSN neuron: soma, vulval presynaptic region and distal axon are labeled with shades of green that match colors in (B-C).

(B) Example of simultaneous calcium imaging of three subcellular compartments of HSN in an immobilized animal.

(C) Average GCaMP signal in each HSN compartment, aligned to HSN calcium peaks in the vulval presynaptic region.

(D) Cartoon depicting split GFP knock-in strain that can be used for cell-specific labeling of *cat*-1/VMAT.

(E) Representative images HSN::CAT-1 in the head (left) and mid-body (right) regions. Images were collected and are displayed using identical settings. Red asterisks indicate gut autofluorescence. Scale bar, 25 um.

(F) **Left:** Cartoon of HSN neuron (red) in a *C. elegans* animal. **Right:** Site of the HSN axotomy: after cutting in this location, the soma is still connected to the vulval presynaptic region, but not the distal axon.

(G) Egg-laying behavior of mock and HSN-axotomized animals. Dots show individual animals. n = 14-15 animals.

(H) Average velocity surrounding native egg-laying events in mock and HSN-axotomized animals. Data display and statistics are similar to Fig. 1G. n = 14-15 animals (126-161 egg laying events). *$p<0.05$, Mann-Whitney U test.

(I) Baseline velocity of indicated conditions and genotypes. Dots show individual animals. n = 14-18 animals. *$p<0.05$, Mann-Whitney U test.

Data are shown as means ± SEM.

See also Figure S5.

Figure 6. Aversive sensory inputs reduce egg-laying via BAG sensory neurons and FLP-17/EGL-6 neuropeptide signaling

(A) Behavioral assay used to measure the effect of high osmolarity on egg-laying behavior. The metric at the bottom is the y-axis in subsequent plots.

(B) Percent eggs laid on indicated osmolarity, compared to control (150 mOsm). Alleles: *tax-2(p691)* and *ocr-2(ak47)*. n = 3 – 4 plates with 10 animals per plate. ****$p<0.0001$, two-factor ANOVA across conditions, with genotype and osmolarity as the two factors; both factors were

significant. In addition, the indicated groups were statistically different with p=0.057, Mann-Whitney U test followed by Benjamini-Hochberg correction for multiple concentrations.

(C) Percent eggs laid on high osmolarity for the indicated genotypes. Alleles: *tax-2(p691)* and *tax-4 (p678)*. Dots show ratios of eggs laid on plates with high osm divided by eggs laid on plates with control osm (measured on paired plates; see Methods). n = 8-13 plates per genotype. ***p<0.0001, Mann-Whitney U tests.

(D) Percent eggs laid on high osmolarity for cell ablation lines. Exact genotypes used are in the key resource table. n = 4-13 plates for each genotype. Statistics were performed as in (C). **p<0.01, Mann-Whitney U tests followed by Bonferroni correction.

(E) Percent eggs laid on high osmolarity for *tax-4* cell-specific rescue lines. Promoters used are listed in key resource table. n = 6-20 plates per genotypes. Statistics were performed as in (C). **p<0.01, Mann-Whitney U tests followed by Bonferroni correction.

(F) Top: Average BAG GCaMP activity, aligned to animals crossing from 150 mOsm agar to 300 mOsm. n=63 animals. **p<0.01, Wilcoxon signed rank test. Bottom: Individual BAG GCaMP traces over the same time frame. Recording gaps (blue) are periods when animals' heads were out of view, but the body was in view such that animal identity could be maintained.

(G) Percent eggs laid on high osmolarity for the indicated genotypes. Alleles: *flp-17*(*n4894*), *flp-10*(*ok2624*), and *egl-6(n4537lf)*. n = 4–8 plates per genotype. Statistics were performed as in (C). *p<0.05 and **p<0.01, Mann-Whitney U tests.

(H) Percent eggs laid on high osmolarity for mock and HSN-axotomized animals (same site of HSN axotomy as shown in Fig. 5F). n = 16-21 animals.

For all panels, statistics were comparing the indicated day-matched groups.

Data are shown as means ± SEM.

See also Figure S6.

STAR METHODS

KEY RESOURCES TABLE

REAGENT or RESOURCE	SOURCE	IDENTIFIER
Antibodies		
Bacterial and Virus Strains		
E. coli: Strain OP50	*Caenorhabditis* Genetics Center	OP50

Chemicals, Peptides, and Recombinant Proteins		
D-(-)-Sorbitol	VWR	Catalog #97062-204
All-trans-retinal	Sigma-Aldrich	Catalog # R2500
Histamine dihydrochloride	Sigma-Aldrich	Catalog # H7250
5-Fluoro-2′-deoxyuridine (FUDR)	Sigma-Aldrich	Catalog # F0503
Critical Commercial Assays		
Deposited Data		
Original data and code related to neural and behavioral data	This paper	https://doi.org/10.5061/dryad.1vhhmgr01
Experimental Models: Organisms/Strains		
C. elegans: wild-type Bristol N2	*Caenorhabditis* Genetics Center	N2
C. elegans: egl-1(n487)	CGC	MT1082
C. elegans: flvEx196(cat-4::invertedCochr,myo-2::mcherry); flvEx197(egl-6::Cre,myo-3::mcherry)	This Paper	SWF502
C. elegans: egl-1(n487); flvEx196(cat-4::invertedCochr,myo-2::mcherry); flvEx197(egl-6::Cre,myo-3::mcherry)	This Paper	SWF632
C. elegans: flvEx288[nlp-3::Gcamp5A (80ng/ul);nlp-3::mscarlet(20ng/ul)]; lite-1(ce314)	This Paper	SWF640
C. elegans: flvEx304[sto-3::nlsGcamp7f(8ng/ul),tdc-1::nlsGcamp7f(10ng/ul), cat4prom68::GCaMP7b(50ng/ul), nlp-3::mscarlet(10ng/ul)]; lite-1(ce314); gur-3(ok2245)	This Paper	SWF691
C. elegans: tph-1(mg280); flvEx196(cat-4::invertedCochr,myo-2::mcherry); flvEx197(egl-6::Cre,myo-3::mcherry)	This Paper	SWF641
C. elegans: nlp-3(n4897); flvEx196(cat-4::invertedCochr,myo-2::mcherry); flvEx197(egl-6::Cre,myo-3::mcherry)	This Paper	SWF915
C. elegans: tph-1(mg280); nlp-3(n4897); flvEx196(cat-4::invertedCochr,myo-2::mcherry); flvEx197(egl-6::Cre,myo-3::mcherry)	This Paper	SWF873

C. elegans: flvEx196(cat-4::invertedCochr,myo-2::mcherry); flvEx197(egl-6::Cre,myo-3::mcherry);unc-17(syb5779 syb5987)	This Paper	SWF1012
C. elegans: egl-21(n476); flvEx196(cat-4::invertedCochr,myo-2::mcherry); flvEx197(egl-6::Cre,myo-3::mcherry)	This Paper	SWF680
C. elegans: HSN::CoChR; HSN specific egl-21 KO: egl-21(n476); kySi61[loxP-egl-21genomic-loxP]; flvEx196(cat-4::invertedCochr,myo-2::mcherry); flvEx197(egl-6::Cre,myo-3::mcherry)	This Paper	SWF717
C. elegans: flp-2(gk1039); flvEx196(cat-4::invertedCochr,myo-2::mcherry);flvEx197(egl-6::Cre,myo-3::mcherry)	This Paper	SWF986
C. elegans: flp-26(gk3015; flvEx196(cat-4::invertedCochr,myo-2::mcherry); flvEx197(egl-6::Cre,myo-3::mcherry)	This Paper	SWF838
C. elegans: flp28(flv11); flvEx196(cat-4::invertedCochr,myo-2::mcherry); flvEx197(egl-6::Cre,myo-3::mcherry)	This Paper	SWF984
C. elegans: flp-2(flv15); flp28(flv11); flvEx196(cat-4::invertedCochr,myo-2::mcherry); flvEx197(egl-6::Cre,myo-3::mcherry)	This Paper	SWF985
C. elegans: flvEx404(Pegl6::HisCl; myo-2p::mcherry)	This Paper	SWF863
C. elegans: flvIs2[tph-1(NSM-specific fragment)::Chrimson, elt-2::mCherry]	Dag et al. (2023)	SWF117
C. elegans: tph-1 (mg280); flvIs2[Ptph-1(NSM-specific fragment)::Chrimson, Pelt-2::mCherry]	Dag et al. (2023)	SWF149
C. elegans: tph-1(mg280); flvIs2[tph-1(NSM-specific fragment)::Chrimson, elt-2::mCherry]; flvEx401[pegl-6::tph-1 cDNA, pmyo-2::mcherry]	This Paper	SWF855
C. elegans: tph-1(mg280); flvIs2[tph-1(NSM-specific fragment)::Chrimson, elt-2::mCherry]; flvEx495[ptph-1::tph-1 cDNA, pmyo-2::mcherry]	This Paper	SWF1011
C. elegans: flvIs2[tph-1(NSM-specific fragment)::Chrimson, elt-2::mCherry]; egl-1(n487)	This Paper	SWF831
C. elegans: flvIs2[tph-1(NSM-specific fragment)::Chrimson, elt-2::mCherry]; mod-5(n822)	This Paper	SWF854

C. elegans: flvIs2[tph-1(NSM-specific fragment)::Chrimson, elt-2::mCherry]; egl-1(n487); mod-5(n822)	This Paper	SWF853
C. elegans: cat-1(syb7239); flvEx478[pegl-6::gfp1-10;pmyo-2::mcherry]	This Paper	SWF991
C. elegans: flvEx201[tag168::mscarlet(5ng/ul); cat4prom68::gfp PCR (10ng/ul)]	This Paper	SWF506
C. elegans: tax-2(p691)	CGC	PR691
C. elegans: ocr-2(ak47)	CGC	CX4535
C. elegans: tax-4 (p678)	CGC	CX13078
C. elegans: -AWB: peIs1715 [str-1p::mCasp-1 + unc-122p::GFP]	CGC	JN1715
C. elegans: -AQR/PQR/URX: qaIs2241[gcy-36::egl-1; gcy-35::GFP; lin-15(+)]	CGC	CX7102
C. elegans: -BAG: kyIs536 (flp-17p::p17 domain of human Caspase3::sl2::gfp; elt-2::GFP); kyIs538 (glb-5p::p12 domain of human Caspase3::sl2::gfp; elt-2::mcherry)	CGC	CX11697
C. elegans: -ASI: oyIs84(gpa-4p::TU#813+gcy-27p::TU#814+gcy-27p::GFP+unc-122p::DsRed) TU#813 and TU#814 are split caspase vectors	CGC	PY7505
C. elegans: -ASJ: mgIs40([daf-28p::nls-GFP]; jxEx100[trx-1::ICE + ofm-1::gfp])	CGC	ZD762
C. elegans: -ASK: qrIs2[sra-9::mCasp1]	CGC	PS6025
C. elegans: -AFD: ttx-1(p767)	CGC	PR767
C. elegans: -AIA: kyEX4745[gcy-28dp::unc-103(gf)::sl2::mCherry, elt-2::mCherry]	CGC	CX14597
C. elegans: -AWC, ASE: ceh-36(ky640); kyIs140 I[Pstr-2::GFP, lin-15(+)]	CGC	CX5922
C. elegans: -AIB: flvEx356[inx-1::unc-103::sl2GFP(30ng/uL); myo-2::mCherry (5ng/uL)]	This Paper	SWF763
C. elegans: -ASK, ASI: oyIs84(gpa-4p::TU#813+gcy-27p::TU#814+gcy-27p::GFP+unc-122p::DsRed) ;qrIs2[sra-9::mCasp1]	This Paper	SWF455
C. elegans: flvEx243[tax-4::tax-4 (50ng/ul), elt-2::gfp (5ng/ul)] ;tax-4 (p678)	This Paper	SWF566

C. elegans: flvEx275[gcy-33::tax-4 (20ng/ul), elt-2::gfp (5ng/ul)] ;tax-4 (p678)	This Paper	SWF615
C. elegans: flvEx497[sra-9::tax-4 (50ng/ul),elt-2::gfp (5ng/ul)] ;tax-4 (p678)	This Paper	SWF1014
C. elegans: flvEx496[srg-47::tax-4 (50ng/ul),elt-2::gfp (5ng/ul)] ;tax-4 (p678)	This Paper	SWF1013
C. elegans: flvEx298[srh-11::tax-4 (50ng/ul),elt-2::gfp (5ng/ul)] ;tax-4 (p678)	This Paper	SWF674
C. elegans: flvEx285[srg-47::tax-4 (30ng/ul), sra-9::tax-4 (30ng/ul),srh-11::tax-4 (30ng/ul),elt-2::gfp (5ng/ul)] ;tax-4 (p678)	This Paper	SWF634
C. elegans: flp-17(n4894)	CGC	MT15933
C. elegans: flp-10(ok2624)	CGC	RB1989
C. elegans: egl-6(n4537lf)	CGC	MT14666
C. elegans: flvEx204(gcy-33::GCamp7b(50ng/ul);myo-3::mcherry(5 ng/ul)))	This Paper	SWF509
C. elegans: nlp-3(n4897);flvIs2[tph-1(short)::Chrimson, elt-2::mCherry]	This Paper	SWF1051
C. elegans: flp-2(flv15); flp28(flv11); flvEx196(cat-4::invertedCochr,myo-2::mcherry);flvEx197(egl-6::Cre,myo-3::mcherry); flvEx529[pcat-4prom68::flp2(genomic)::venus (5ng/ul PCR);pcat-4prom68::FLP-28 cDNA::venus (5ng/ul PCR); elt-2::gfp (5ng/ul)]	This Paper	SWF1056
Software and Algorithms		
MATLAB (2021)	Mathworks	https://www.mathworks.com
GraphPad Prism (v10)	GraphPad Software	https://www.graphpad.com
R Studio	RStudio	https://rstudio.com
Fiji (v1.52)	NIH	https://fiji.sc/
Streampix (v7.0)	Norpix	https://www.norpix.com
Adobe Illustrator	Adobe	https://www.adobe.com
Tracking Scope image analysis	Cermak et al. (2020)	https://bitbucket.org/natecermak/wormimageanalysisr/src/master/

Other		
SP-20000M-USB3 CMOS camera	JAI	N/A
Micro-NIKKOR 55mm f/2.8 lens	Nikon	N/A
10x25 White Panel LED backlight, 24VDC	Metaphase Technologies	Cat#MS-BL10X25-W-24-ILD-PS
Precision LED Spot Light, 625nm, 40W, Type H	Mightex	Cat#BLS-PLS-0625-030-40-S
BioLED Light Source Control Module	Mightex	Cat#BLS-13000-1
Zyla 4.2 Plus sCMOS camera	Andor	N/A
Ti-E Inverted Microscope	Nikon	N/A

RESOURCE AVAILABILITY

Lead Contact

Further information and requests for resources and reagents should be directed to and will be fulfilled by the lead contact, Steven Flavell (flavell@mit.edu).

Materials Availability

All plasmids, strains, and other reagents generated in this study are freely available upon request.

Data and Code Availability

- Data: Behavioral and neural data related to Figures 2 and Figure 6 have been deposited at Dryad. DOIs are listed in the key resources table. All other data reported in this paper are freely available upon request.
- Code: Original code for neuron tracking has been deposited at Dryad. DOIs are listed in the key resources table.
- Any additional information required to reanalyze the data reported in this paper is available from the Lead Contact upon request.

EXPERIMENTAL MODEL AND STUDY PARTICIPANT DETAILS

C. elegans

C. elegans Bristol strain N2 was used as wild-type. All wild-type, mutant and transgenic strains used are listed in the key resources table. Animals were maintained on NGM agar plates seeded with E. coli OP50 bacteria strain and kept at 22°C, 40% humidity. One day-old adults were used

for all experiments. For genetic crosses, genotypes were confirmed by PCR and/or sequencing. Transgenic animals were generated either by injecting DNA with fluorescent co-injection markers into the gonads of young adult hermaphrodites, CRISPR/Cas9 genome editing or mosSCI insertion.

METHOD DETAILS

Plasmids and Promoters

Plasmid backbones: *C. elegans* codon-optimized GCaMP7b and GCaMP7f open reading frames were synthesized and inserted into the pSM vector. The intersectional promoters, consisting of the inverted/floxed vector and the Cre vector were previously described (Flavell et al., 2013). The HisCl1 plasmid was previously described (Pokala et al., 2014). For *tax-4* rescue, we used the previously described *tax-4* cDNA [69], but moved it into a pSM-t2a-GFP vector backbone for expression. For *tph-1* rescue, we used the KZ1290.21.1 cDNA, which we subcloned into the pSM vector.

Promoters used in this study: *egl-6* (Flavell et al., 2013), *cat-4* (full length, 4kB immediately upstream of *cat-4* start codon), *cat-4prom68* [70], *sto-3* (Ji et al., 2021). The NSM-specific promoter was a 158 bp fragment of *tph-1* promoter, validated to be NSM-specific in our previous work through GFP expression and Ribotagging analysis (Rhoades et al., 2019). In addition, we showed that the resulting NSM::Chrimson line used here has no light-induced egg-laying even at maximum light intensities tested (Dag et al., 2023), further confirming that it confers no HSN-specific expression.

New alleles generated in this study

The *egl-21* cell-specific deletion strain was constructed in an *egl-21(n476)* mutant background. For the mosSCI insertion, the *egl-21* genomic region (spanning entire genomic region up to adjacent genes in both directions) was inserted into the mosSCI insertion site on chromosome IV [71]. LoxP sites that we inserted into the *egl-21* single-copy rescue allow for Cre-dependent deletion of exons 2 through 5 of the *egl-21* gene, which is the majority of the coding sequence.

The conditional knockout allele of *unc-17* was constructed via iterative rounds of CRISPR/Cas9 genome editing. One loxP site was inserted ~250bp after the end of the *unc-17* 3'UTR. Another loxP site was inserted in the intron before the last coding exon (which encodes the majority of the UNC-17 protein). We found that pan-neuronal Cre expression in this strain gave rise to animals with an Unc phenotype, validating that the loxP sites work effectively.

The cell-specific fluorescent labeling strain for *cat-1* was generated via CRISPR/Cas9 genome editing. Three tandem repeats of the GFP11 sequence separated by short linker sequences (gly-gly-ser-gly-gly) were inserted immediately before the *cat-1* stop codon.

Multi-animal behavioral recordings

Multi-animal recordings of *C. elegans* locomotion were conducted as previously described (Rhoades et al., 2019). One day old adult animals of the indicated genotypes were transferred to NGM plates with or without OP50 bacteria. For animals that were fasted, animals were transferred to NGM plates without OP50 for three hours prior to recording. All animals were recorded using Streampix software at 3 fps. JAI SP-20000M-USB3 CMOS cameras (5120x3840, mono) with Nikon Micro-NIKKOR 55mm f/2.8 were used. White-panel LEDs (Metaphase) provided backlighting. Videos were analyzed using previously-described custom MATLAB scripts (Rhoades et al., 2019). For optogenetic stimulation, light was supplied from a 470nm (for CoChR; 0.5 mW/mm2) or 625nm (for Chrimson; 0.6 mW/mm2 unless otherwise specified) Mightex LED at defined times in the video.

Single-animal behavioral recordings

For joint recordings of egg-laying and locomotion, we used previously described custom-built single worm tracking microscopes (Cermak et al., 2020). These custom microscopes have a live-tracking function that permits long-term recording of single moving animals. L4s animals were picked 16-20 hours before the recording day. On the day of the recording, animals were transferred to NGM plates seeded with OP50 (1:20 dilution of saturated culture) the day before the recording (thin bacterial lawns are a requirement for the live-tracking function on the microscopes). LabView software controlled the microscope and acquired the images. Data were then analyzed in R Studio and MATLAB. For optogenetic stimulation, 532nm laser light was supplied at defined times at an intensity of 250 uW/mm^2.

HSN Axotomy

Laser axotomy was performed as previously described [72] with a few modifications. L4 stage transgenic animals were transferred to a 3% agarose pad and immobilized with 2.5mM levamisole in M9 buffer. Animals were visualized with a Nikon Eclipse 80i microscope, 100x Plan Apo VC lens (1.4 NA), Andor Zyla sCMOS camera and a Leica EL6000 light source. HSN axons were severed anterior to the vulval presynaptic region and before they extend to the ventral nerve cord using a 435nm nitrogen pulsed MicroPoint laser fired at 20 Hz. Both HSNL and HSNR axons were sequentially severed by gently rolling the animal from one side to the other after the first axotomy. To facilitate rolling, grooved agarose pads were stamped with a portion of a vinyl record [73]. 'mock' control animals underwent the same immobilization and rolling protocol but were not axotomized. Both mock and axotomized animals were immediately recovered in M9 buffer and transferred to OP50 seeded NGM plates for behavioral analyses 20 hours later. For control axotomies, the laser was fired using the same settings that were used for the real axotomy, but it was targeted adjacent to the HSN neurite and confirmed to not visibly damage HSN, based on HSN fluorescence.

Freely-moving HSN and BAG Calcium Imaging

HSN calcium imaging in freely-moving animals was conducted as previously described (Rhoades et al., 2019) with a few small modifications. Animals were mounted on flat agar, with freshly seeded OP50 bacterial food. They were enclosed in a small chamber with a rubber gasket and cover glass and GCaMP/mCherry data was recorded at 10 fps (with 10ms exposure times). Agar was either normal 150 mOsm or 300 mOsm (due to addition of sorbitol), as described in the text and figure legends. Imaging was performed with a 4x/0.2NA objective and data was acquired on two Andor Zyla 4.2 Plus sCMOS cameras. A Cairn TwinCam beam splitter was used to separate GCaMP and mCherry signals. The GCaMP/mCherry imaging at 10 fps was interleaved with 5 fps brightfield imaging, achieved via NI-DAQ triggering of different light sources using the NIS Elements Illumination Sequence module. For data analysis, the HSN soma was tracked (using the bright mCherry signal) using custom ImageJ macros. After cell positions were determined by ImageJ tracking, the GCaMP and mCherry signals were extracted from each ROI at each time point. Background was subtracted from each signal and then the ratio of the two background-subtracted fluorescence measurements was taken. Time points of egg-laying were manually determined from the brightfield images.

For BAG calcium imaging, animals were placed on agar that was fused. This was done by first pouring a normal osmolarity NGM pad on a microscope slide, then slicing it to make a flat edge on one side. 300 mOsm agar (adjusted with sorbitol) was then poured next to the first NGM pad and allowed to dry. Animals were picked to this flat agar surface and imaged as described above. GCaMP data was recorded at 10 fps (with 10ms exposure times). Custom ImageJ tracking scripts were used to track and quantify BAG GCaMP fluorescence.

Immobilized Calcium Imaging

Calcium imaging of HSN and RIB, as well as different HSN compartments, in immobilized animals was conducted on a previously described spinning disk confocal microscope (Ji et al., 2021). Animals were mounted on 5% agar with 0.05um beads for immobilization [74]. They were imaged using a 20X/0.95 objective coupled to a 5000 rpm Yokogawa CSU-X1 spinning disk unit with a Borealis upgrade. Z-stacks were collected with NIS Elements software. For data analysis, data were converted to maximum intensity projections (RIB and HSN were typically in different z-planes), ROIs were manually drawn around the somas of RIB and HSN, and then background-subtracted intensities within the ROIs were calculated.

Imaging of CAT-1::GFP puncta

CAT-1::GFP puncta in HSN were imaged on a spinning disk confocal microscope that has been previously described [6]. Imaging of the head and vulval regions was conducted using identical camera settings and entire z-stacks were collected spanning the depth of the animal's body, with exposure times set such that there were no saturated pixels. In addition, a longer exposure z-stack was collected for the head region to provide a higher SNR image of dim signals in the head.

Egg Counting Assays and Osmolarity Exposure

NGM plates with varying osmolarities were used for egg-laying assays. Sorbitol was used to increase the osmolarity in the NGM plates to desired osmolarity (300-450 mOSm), and added together with $CaCl_2$ and KPO_4 buffer to the NGM agar. The day before the assay, assay plates were seeded with 200 ul OP50 per plate, and lids were left open for 20 minutes in the biosafety hood to allow them to dry. L4s animals were picked to OP50-seeded NGM plates the day before the assays and grown for 20-24 hours to become gravid adults. On the day of the experiment, adult animals were transferred onto seeded control or high osmolarity plates (10 animals per plate), and were left to lay eggs for an hour. After an hour, animals were removed from assay plates and the number of eggs laid was counted. The percentage of egg laid was calculated by the number of eggs laid on high osmolarity plates divided by the number of eggs laid on control plates.

Exploration assays

Exploration assays that provide a reliable measure of roaming versus dwelling behavior were performed as previously described (Flavell et al., 2013) with minor modifications. Single L4 animals were picked to NGM plates with OP50 bacteria seeded 1 day prior. They were then left to explore the plates for 16 hours, after which the plate was superimposed on a transparent grid and the number grid squares that the animal tracks traversed was quantified. In some experiments (as indicated in the text), animals were mounted as adults on plates and allowed to explore for 3 hours, and then the number of squares was counted.

QUANTIFICATION AND STATISTICAL ANALYSES

Descriptions of statistical tests and group sizes are provided in figure legends. In addition, definitions of center and dispersion and precision measures are also in the figure legends. Here, we provide an overview of statistical methods that were used in multiple places in the paper, providing additional information not in the figure legends.

For all HSN optogenetics experiments conducted using single-worm recordings (i.e. those that include both velocity and egg-laying quantification), we used the following statistical procedure. First, for each individual optogenetic trial we determined the increase in velocity during optogenetic stimulation, compared to pre-light baseline (-2 to 0 min before each stimulus). We then averaged this for all trials in a given animal to get that animal's average increase in velocity caused by optogenetic stimulation. This n (# of animals) was the n used in statistical analyses. To compare across genotypes, we performed a Mann-Whitney U test comparing the velocity increase in the group of control animals to the velocity increase in the treatment (e.g. mutant) group. For statistical tests on the egg-laying effects, we performed a similar analysis, but just on the mean egg-laying rate during optogenetic stimulation (since the

baseline is essentially zero). In many analyses, the appropriate control group was HSN::CoChR +ATR animals. The single worm tracker is low throughput (one animal is recorded over 3 or 6 hours), so we tested whether it was appropriate to pool animals of this control group across days. We did this by taking all of our recordings and performing a one-factor ANOVA where 'recording date' was the factor (i.e. testing whether animals' HSN-induced velocity increase was dependent on recording date). We found that there was no significant effect of recording date (Fig. S1B; $F=1.162$; $p=0.3738$), so we pooled these animals and used them as the comparison group for several treatment groups recorded over the same overall time period.

For HSN optogenetics experiments conducted using multi-worm tracking, we only analyzed data over one single optogenetics trial per animal. We computed the change in speed (compared to baseline) for each animal and then compared the magnitude of the speed change in mutant animals to day-matched controls (using an 'n' that is equal to the number of animals assayed) with a Mann-Whitney U test.

For analyses of velocity surrounding spontaneous egg-laying events, data were recorded on single-worm trackers. Analysis was conducted very similarly to the HSN optogenetics single worm tracker analysis. For each egg-laying event, we determined the velocity increase right before the egg-laying event by computing the difference between velocity during egg-laying (from -15s to 0s before egg-laying event) and a preceding baseline period (-5 to -3 min before egg-laying event). We then averaged this value across all observations in each animal to obtain per-animal averages. To compare treatment groups, we performed a Mann-Whitney U test to compare the two respective groups of animals. In many cases, the appropriate control group was wild-type (N2). Again based on the low-throughput nature of this single-worm recording assay, we asked whether it was possible to pool wild-type animals' data across days. We again used a one-factor ANOVA where the factor was 'recording date' and found no effect. This suggested that it was valid to pool wild-type animals and compare them to treatment groups recorded over the same overall time period.

For egg-laying assays where we examined the influence of osmolarity on egg-laying, statistics were performed as follows: To obtain a single biological replicate (shown as individual dots in Fig. 6), animals were staged as L4s the day before the assay on a single OP50 growth plate. Then, the next day animals from a single growth plate were split onto one normal osmolarity plate and one high osmolarity plate (10 animals per plate). Egg-laying over one hour was counted for each plate. Therefore, from each staged L4 plate, we had paired measurements of egg-laying at each osmolarity level. We then took the ratio of these values (this is what is shown as dots in Fig. 6). We obtained distributions of these ratio values for each genotype based on multiple replicates and ran a Mann-Whitney U test, comparing day-matched wild-type controls to the mutant/transgenic of interest. For Fig. 6B, which was an initial trial that tested multiple osmolarity concentrations, we instead ran a two-factor ANOVA (with genotype and osmolarity level as the two factors) on raw egg-laying rates in each condition, as well as Bonferroni-corrected Mann-Whitney U tests comparing WT versus mutants at each of the four osmolarity levels. For the genotype of interest from Fig. 6B (*tax-2*), additional experiments were

run and statistics for those experiments were performed using the above approach (Fig. 6C shows independent data for *tax-2*, not overlapping with the data in Fig. 6B).

When running parametric tests, including the ANOVAs described in this section and all t-tests in the manuscript, the D'Agostino-Pearson test for normality was used to test that the distributions were normally distributed. In addition, multiple comparison corrections were conducted where appropriate, as stated in figure legends. Statistics were computed using MATLAB and Graphpad Prism.

REFERENCES

1. Bucher, D., Taylor, A.L., and Marder, E. (2006). Central pattern generating neurons simultaneously express fast and slow rhythmic activities in the stomatogastric ganglion. J. Neurophysiol. *95*, 3617–3632. 10.1152/jn.00004.2006.

2. Weimann, J.M., and Marder, E. (1994). Switching neurons are integral members of multiple oscillatory networks. Curr. Biol. CB *4*, 896–902. 10.1016/s0960-9822(00)00199-8.

3. Atanas, A.A., Kim, J., Wang, Z., Bueno, E., Becker, M., Kang, D., Park, J., Estrem, C., Kramer, T.S., Baskoylu, S., et al. (2022). Brain-wide representations of behavior spanning multiple timescales and states in C. elegans. 2022.11.11.516186. 10.1101/2022.11.11.516186.

4. Fisher, Y.E. (2022). Flexible navigational computations in the Drosophila central complex. Curr. Opin. Neurobiol. *73*, 102514. 10.1016/j.conb.2021.12.001.

5. Fusi, S., Miller, E.K., and Rigotti, M. (2016). Why neurons mix: high dimensionality for higher cognition. Curr. Opin. Neurobiol. *37*, 66–74. 10.1016/j.conb.2016.01.010.

6. Ji, N., Madan, G.K., Fabre, G.I., Dayan, A., Baker, C.M., Kramer, T.S., Nwabudike, I., and Flavell, S.W. (2021). A neural circuit for flexible control of persistent behavioral states. eLife *10*, e62889. 10.7554/eLife.62889.

7. Svensson, E., Apergis-Schoute, J., Burnstock, G., Nusbaum, M.P., Parker, D., and Schiöth, H.B. (2018). General Principles of Neuronal Co-transmission: Insights From Multiple Model Systems. Front. Neural Circuits *12*, 117. 10.3389/fncir.2018.00117.

8. Florman, J.T., and Alkema, M.J. (2022). Co-transmission of neuropeptides and monoamines choreograph the C. elegans escape response. PLoS Genet. *18*, e1010091. 10.1371/journal.pgen.1010091.

9. Huo, J., Xu, T., Polat, M., Zhang, X., and Wen, Q. (2023). Hierarchical behavior control by a single class of interneurons. 2023.03.13.532397. 10.1101/2023.03.13.532397.

10. Sordillo, A., and Bargmann, C.I. (2021). Behavioral control by depolarized and hyperpolarized states of an integrating neuron. eLife *10*, e67723. 10.7554/eLife.67723.

11. Tritsch, N.X., Ding, J.B., and Sabatini, B.L. (2012). Dopaminergic neurons inhibit striatal output through non-canonical release of GABA. Nature *490*, 262–266. 10.1038/nature11466.

12. Hendricks, M., Ha, H., Maffey, N., and Zhang, Y. (2012). Compartmentalized calcium dynamics in a C. elegans interneuron encode head movement. Nature *487*, 99–103. 10.1038/nature11081.

13. Stuyt, G., Godenzini, L., and Palmer, L.M. (2022). Local and Global Dynamics of Dendritic Activity in the Pyramidal Neuron. Neuroscience *489*, 176–184. 10.1016/j.neuroscience.2021.07.008.

14. Cook, S.J., Jarrell, T.A., Brittin, C.A., Wang, Y., Bloniarz, A.E., Yakovlev, M.A., Nguyen, K.C.Q., Tang, L.T.-H., Bayer, E.A., Duerr, J.S., et al. (2019). Whole-animal connectomes of both Caenorhabditis elegans sexes. Nature *571*, 63–71. 10.1038/s41586-019-1352-7.

15. White, J.G., Southgate, E., Thomson, J.N., and Brenner, S. (1986). The structure of the nervous system of the nematode Caenorhabditis elegans. Philos. Trans. R. Soc. Lond. B. Biol. Sci. *314*, 1–340.

16. Witvliet, D., Mulcahy, B., Mitchell, J.K., Meirovitch, Y., Berger, D.R., Wu, Y., Liu, Y., Koh, W.X., Parvathala, R., Holmyard, D., et al. (2021). Connectomes across development reveal principles of brain maturation. Nature *596*, 257–261. 10.1038/s41586-021-03778-8.

17. de Bono, M., and Maricq, A.V. (2005). Neuronal substrates of complex behaviors in C. elegans. Annu. Rev. Neurosci. *28*, 451–501. 10.1146/annurev.neuro.27.070203.144259.

18. Cermak, N., Yu, S.K., Clark, R., Huang, Y.-C., Baskoylu, S.N., and Flavell, S.W. (2020). Whole-organism behavioral profiling reveals a role for dopamine in state-dependent motor program coupling in C. elegans. eLife *9*. 10.7554/eLife.57093.

19. Collins, K.M., Bode, A., Fernandez, R.W., Tanis, J.E., Brewer, J.C., Creamer, M.S., and Koelle, M.R. (2016). Activity of the C. elegans egg-laying behavior circuit is controlled by competing activation and feedback inhibition. eLife *5*. 10.7554/eLife.21126.

20. Hardaker, L.A., Singer, E., Kerr, R., Zhou, G., and Schafer, W.R. (2001). Serotonin modulates locomotory behavior and coordinates egg-laying and movement in Caenorhabditis elegans. J. Neurobiol. *49*, 303–313. 10.1002/neu.10014.

21. Nagy, S., Huang, Y.-C., Alkema, M.J., and Biron, D. (2015). Caenorhabditis elegans exhibit a coupling between the defecation motor program and directed locomotion. Sci. Rep. *5*, 17174. 10.1038/srep17174.

22. Flavell, S.W., and Gordus, A. (2022). Dynamic functional connectivity in the static connectome of Caenorhabditis elegans. Curr. Opin. Neurobiol. *73*, 102515. 10.1016/j.conb.2021.12.002.

23. Schafer, W.F. (2006). Genetics of egg-laying in worms. Annu. Rev. Genet. *40*, 487–509. 10.1146/annurev.genet.40.110405.090527.

24. Taylor, S.R., Santpere, G., Weinreb, A., Barrett, A., Reilly, M.B., Xu, C., Varol, E., Oikonomou, P., Glenwinkel, L., McWhirter, R., et al. (2021). Molecular topography of an entire nervous system. Cell *184*, 4329-4347.e23. 10.1016/j.cell.2021.06.023.

25. Emtage, L., Aziz-Zaman, S., Padovan-Merhar, O., Horvitz, H.R., Fang-Yen, C., and Ringstad, N. (2012). IRK-1 potassium channels mediate peptidergic inhibition of Caenorhabditis elegans serotonin neurons via a G(o) signaling pathway. J. Neurosci. Off. J. Soc. Neurosci. *32*, 16285–16295. 10.1523/JNEUROSCI.2667-12.2012.

26. Ringstad, N., and Horvitz, H.R. (2008). FMRFamide neuropeptides and acetylcholine synergistically inhibit egg-laying by C. elegans. Nat. Neurosci. *11*, 1168–1176. 10.1038/nn.2186.

27. Ravi, B., Garcia, J., and Collins, K.M. (2018). Homeostatic Feedback Modulates the Development of Two-State Patterned Activity in a Model Serotonin Motor Circuit in Caenorhabditis elegans. J. Neurosci. Off. J. Soc. Neurosci. *38*, 6283–6298. 10.1523/JNEUROSCI.3658-17.2018.

28. Brewer, J.C., Olson, A.C., Collins, K.M., and Koelle, M.R. (2019). Serotonin and neuropeptides are both released by the HSN command neuron to initiate Caenorhabditis elegans egg laying. PLoS Genet. *15*, e1007896. 10.1371/journal.pgen.1007896.

29. Aprison, E.Z., and Ruvinsky, I. (2019). Dynamic Regulation of Adult-Specific Functions of the Nervous System by Signaling from the Reproductive System. Curr. Biol. CB *29*, 4116-4123.e3. 10.1016/j.cub.2019.10.011.

30. Flavell, S.W., Pokala, N., Macosko, E.Z., Albrecht, D.R., Larsch, J., and Bargmann, C.I. (2013). Serotonin and the neuropeptide PDF initiate and extend opposing behavioral states in C. elegans. Cell *154*, 1023–1035. 10.1016/j.cell.2013.08.001.

31. Klapoetke, N.C., Murata, Y., Kim, S.S., Pulver, S.R., Birdsey-Benson, A., Cho, Y.K., Morimoto, T.K., Chuong, A.S., Carpenter, E.J., Tian, Z., et al. (2014). Independent optical excitation of distinct neural populations. Nat. Methods *11*, 338–346. 10.1038/nmeth.2836.

32. Conradt, B., and Horvitz, H.R. (1999). The TRA-1A sex determination protein of C. elegans regulates sexually dimorphic cell deaths by repressing the egl-1 cell death activator gene. Cell *98*, 317–327. 10.1016/s0092-8674(00)81961-3.

33. Zhang, M., Chung, S.H., Fang-Yen, C., Craig, C., Kerr, R.A., Suzuki, H., Samuel, A.D.T., Mazur, E., and Schafer, W.R. (2008). A self-regulating feed-forward circuit controlling C. elegans egg-laying behavior. Curr. Biol. CB *18*, 1445–1455. 10.1016/j.cub.2008.08.047.

34. Zang, K.E., Ho, E., and Ringstad, N. (2017). Inhibitory peptidergic modulation of C. elegans serotonin neurons is gated by T-type calcium channels. eLife *6*, e22771. 10.7554/eLife.22771.

35. Gordus, A., Pokala, N., Levy, S., Flavell, S.W., and Bargmann, C.I. (2015). Feedback from network states generates variability in a probabilistic olfactory circuit. Cell *161*, 215–227. 10.1016/j.cell.2015.02.018.

36. Kato, S., Kaplan, H.S., Schrödel, T., Skora, S., Lindsay, T.H., Yemini, E., Lockery, S., and Zimmer, M. (2015). Global brain dynamics embed the motor command sequence of Caenorhabditis elegans. Cell *163*, 656–669. 10.1016/j.cell.2015.09.034.

37. Uzel, K., Kato, S., and Zimmer, M. (2022). A set of hub neurons and non-local connectivity features support global brain dynamics in C. elegans. Curr. Biol. CB *32*, 3443-3459.e8. 10.1016/j.cub.2022.06.039.

38. Pereira, L., Kratsios, P., Serrano-Saiz, E., Sheftel, H., Mayo, A.E., Hall, D.H., White, J.G., LeBoeuf, B., Garcia, L.R., Alon, U., et al. (2015). A cellular and regulatory map of the cholinergic nervous system of C. elegans. eLife *4*, e12432. 10.7554/eLife.12432.

39. Rand, J.B., and Russell, R.L. (1984). Choline acetyltransferase-deficient mutants of the nematode Caenorhabditis elegans. Genetics *106*, 227–248. 10.1093/genetics/106.2.227.

40. Alfonso, A., Grundahl, K., Duerr, J.S., Han, H.P., and Rand, J.B. (1993). The Caenorhabditis elegans unc-17 gene: a putative vesicular acetylcholine transporter. Science *261*, 617–619. 10.1126/science.8342028.

41. Beets, I., Zels, S., Vandewyer, E., Demeulemeester, J., Caers, J., Baytemur, E., Schafer, W.R., Vértes, P.E., Mirabeau, O., and Schoofs, L. (2022). System-wide mapping of neuropeptide-GPCR interactions in C. elegans. 2022.10.30.514428. 10.1101/2022.10.30.514428.

42. Ripoll-Sánchez, L., Watteyne, J., Sun, H., Fernandez, R., Taylor, S.R., Weinreb, A., Hammarlund, M., Miller, D.M., Hobert, O., Beets, I., et al. (2022). The neuropeptidergic connectome of C. elegans. 2022.10.30.514396. 10.1101/2022.10.30.514396.

43. Jacob, T.C., and Kaplan, J.M. (2003). The EGL-21 carboxypeptidase E facilitates acetylcholine release at Caenorhabditis elegans neuromuscular junctions. J. Neurosci. Off. J. Soc. Neurosci. *23*, 2122–2130. 10.1523/JNEUROSCI.23-06-02122.2003.

44. Chen, D., Taylor, K.P., Hall, Q., and Kaplan, J.M. (2016). The Neuropeptides FLP-2 and PDF-1 Act in Concert To Arouse Caenorhabditis elegans Locomotion. Genetics *204*, 1151–1159. 10.1534/genetics.116.192898.

45. Pokala, N., Liu, Q., Gordus, A., and Bargmann, C.I. (2014). Inducible and titratable silencing of Caenorhabditis elegans neurons in vivo with histamine-gated chloride channels. Proc. Natl. Acad. Sci. U. S. A. *111*, 2770–2775. 10.1073/pnas.1400615111.

46. Jafari, G., Xie, Y., Kullyev, A., Liang, B., and Sze, J.Y. (2011). Regulation of extrasynaptic 5-HT by serotonin reuptake transporter function in 5-HT-absorbing neurons underscores adaptation behavior in Caenorhabditis elegans. J. Neurosci. Off. J. Soc. Neurosci. *31*, 8948–8957. 10.1523/JNEUROSCI.1692-11.2011.

47. Ranganathan, R., Sawin, E.R., Trent, C., and Horvitz, H.R. (2001). Mutations in the Caenorhabditis elegans serotonin reuptake transporter MOD-5 reveal serotonin-dependent and -independent activities of fluoxetine. J. Neurosci. Off. J. Soc. Neurosci. *21*, 5871–5884. 10.1523/JNEUROSCI.21-16-05871.2001.

48. Sawin, E.R., Ranganathan, R., and Horvitz, H.R. (2000). C. elegans locomotory rate is modulated by the environment through a dopaminergic pathway and by experience through a serotonergic pathway. Neuron *26*, 619–631.

49. Rhoades, J.L., Nelson, J.C., Nwabudike, I., Yu, S.K., McLachlan, I.G., Madan, G.K., Abebe, E., Powers, J.R., Colón-Ramos, D.A., and Flavell, S.W. (2019). ASICs Mediate Food Responses in an Enteric Serotonergic Neuron that Controls Foraging Behaviors. Cell *176*, 85-97.e14. 10.1016/j.cell.2018.11.023.

50. Dag, U., Nwabudike, I., Kang, D., Gomes, M.A., Kim, J., Atanas, A.A., Bueno, E., Estrem, C., Pugliese, S., Wang, Z., et al. (2023). Dissecting the functional organization of the C. elegans serotonergic system at whole-brain scale. Cell *186*, 2574-2592.e20. 10.1016/j.cell.2023.04.023.

51. Gürel, G., Gustafson, M.A., Pepper, J.S., Horvitz, H.R., and Koelle, M.R. (2012). Receptors and other signaling proteins required for serotonin control of locomotion in Caenorhabditis elegans. Genetics *192*, 1359–1371. 10.1534/genetics.112.142125.

52. Duerr, J.S., Frisby, D.L., Gaskin, J., Duke, A., Asermely, K., Huddleston, D., Eiden, L.E., and Rand, J.B. (1999). The cat-1 gene of Caenorhabditis elegans encodes a vesicular monoamine transporter required for specific monoamine-dependent behaviors. J. Neurosci. Off. J. Soc. Neurosci. *19*, 72–84.

53. Fenk, L.A., and de Bono, M. (2015). Environmental CO2 inhibits Caenorhabditis elegans egg-laying by modulating olfactory neurons and evokes widespread changes in neural activity. Proc. Natl. Acad. Sci. U. S. A. *112*, E3525-3534. 10.1073/pnas.1423808112.

54. Liu, Z., Kariya, M.J., Chute, C.D., Pribadi, A.K., Leinwand, S.G., Tong, A., Curran, K.P., Bose, N., Schroeder, F.C., Srinivasan, J., et al. (2018). Predator-secreted sulfolipids induce defensive responses in C. elegans. Nat. Commun. *9*, 1128. 10.1038/s41467-018-03333-6.

55. Teshiba, E., Miyahara, K., and Takeya, H. (2016). Glucose-induced abnormal egg-laying rate in Caenorhabditis elegans. Biosci. Biotechnol. Biochem. *80*, 1436–1439. 10.1080/09168451.2016.1158634.

56. Trent, C., Tsuing, N., and Horvitz, H.R. (1983). Egg-laying defective mutants of the nematode Caenorhabditis elegans. Genetics *104*, 619–647. 10.1093/genetics/104.4.619.

57. Yu, J., Yang, W., Liu, H., Hao, Y., and Zhang, Y. (2017). An Aversive Response to Osmotic Upshift in Caenorhabditis elegans. eNeuro *4*, ENEURO.0282-16.2017. 10.1523/ENEURO.0282-16.2017.

58. Ferkey, D.M., Sengupta, P., and L'Etoile, N.D. (2021). Chemosensory signal transduction in Caenorhabditis elegans. Genetics *217*, iyab004. 10.1093/genetics/iyab004.

59. Hallem, E.A., and Sternberg, P.W. (2008). Acute carbon dioxide avoidance in Caenorhabditis elegans. Proc. Natl. Acad. Sci. U. S. A. *105*, 8038–8043. 10.1073/pnas.0707469105.

60. Zimmer, M., Gray, J.M., Pokala, N., Chang, A.J., Karow, D.S., Marletta, M.A., Hudson, M.L., Morton, D.B., Chronis, N., and Bargmann, C.I. (2009). Neurons detect increases and decreases in oxygen levels using distinct guanylate cyclases. Neuron *61*, 865–879. 10.1016/j.neuron.2009.02.013.

61. Ringstad, N., and Horvitz, H.R. (2008). FMRFamide neuropeptides and acetylcholine synergistically inhibit egg-laying by C. elegans. Nat. Neurosci. *11*, 1168–1176. 10.1038/nn.2186.

62. Ghai, K., Zelinka, C., and Fischer, A.J. (2009). Serotonin released from amacrine neurons is scavenged and degraded in bipolar neurons in the retina. J. Neurochem. *111*, 1–14. 10.1111/j.1471-4159.2009.06270.x.

63. Lebrand, C., Cases, O., Adelbrecht, C., Doye, A., Alvarez, C., El Mestikawy, S., Seif, I., and Gaspar, P. (1996). Transient uptake and storage of serotonin in developing thalamic neurons. Neuron *17*, 823–835. 10.1016/s0896-6273(00)80215-9.

64. Zhang, Y., Lu, H., and Bargmann, C.I. (2005). Pathogenic bacteria induce aversive olfactory learning in Caenorhabditis elegans. Nature *438*, 179–184. 10.1038/nature04216.

65. Gendrel, M., Atlas, E.G., and Hobert, O. (2016). A cellular and regulatory map of the GABAergic nervous system of C. elegans. eLife *5*, e17686. 10.7554/eLife.17686.

66. Dag, U., Nwabudike, I., Kang, D., Gomes, M.A., Kim, J., Atanas, A.A., Bueno, E., Estrem, C., Pugliese, S., Wang, Z., et al. (2023). Dissecting the Functional Organization of the C. elegans Serotonergic System at Whole-Brain Scale. BioRxiv Prepr. Serv. Biol., 2023.01.15.524132. 10.1101/2023.01.15.524132.

67. Unger, E.K., Keller, J.P., Altermatt, M., Liang, R., Matsui, A., Dong, C., Hon, O.J., Yao, Z., Sun, J., Banala, S., et al. (2020). Directed Evolution of a Selective and Sensitive Serotonin Sensor via Machine Learning. Cell *183*, 1986-2002.e26. 10.1016/j.cell.2020.11.040.

68. Wan, J., Peng, W., Li, X., Qian, T., Song, K., Zeng, J., Deng, F., Hao, S., Feng, J., Zhang, P., et al. (2021). A genetically encoded sensor for measuring serotonin dynamics. Nat. Neurosci. *24*, 746–752. 10.1038/s41593-021-00823-7.

69. Macosko, E.Z., Pokala, N., Feinberg, E.H., Chalasani, S.H., Butcher, R.A., Clardy, J., and Bargmann, C.I. (2009). A hub-and-spoke circuit drives pheromone attraction and social behaviour in C. elegans. Nature *458*, 1171–1175. 10.1038/nature07886.

70. Lloret-Fernández, C., Maicas, M., Mora-Martínez, C., Artacho, A., Jimeno-Martín, Á., Chirivella, L., Weinberg, P., and Flames, N. (2018). A transcription factor collective defines the HSN serotonergic neuron regulatory landscape. eLife *7*, e32785. 10.7554/eLife.32785.

71. Frøkjaer-Jensen, C., Davis, M.W., Hopkins, C.E., Newman, B.J., Thummel, J.M., Olesen, S.-P., Grunnet, M., and Jorgensen, E.M. (2008). Single-copy insertion of transgenes in Caenorhabditis elegans. Nat. Genet. *40*, 1375–1383. 10.1038/ng.248.

72. Byrne, A.B., Edwards, T.J., and Hammarlund, M. (2011). In vivo laser axotomy in C. elegans. J. Vis. Exp. JoVE, 2707. 10.3791/2707.

73. Rivera Gomez, K., and Schvarzstein, M. (2018). Immobilization of nematodes for live imaging using an agarose pad produced with a Vinyl Record. MicroPublication Biol. *2018*. 10.17912/QG0J-VT85.

74. Kim, E., Sun, L., Gabel, C.V., and Fang-Yen, C. (2013). Long-term imaging of Caenorhabditis elegans using nanoparticle-mediated immobilization. PloS One *8*, e53419. 10.1371/journal.pone.0053419.

Figure 1

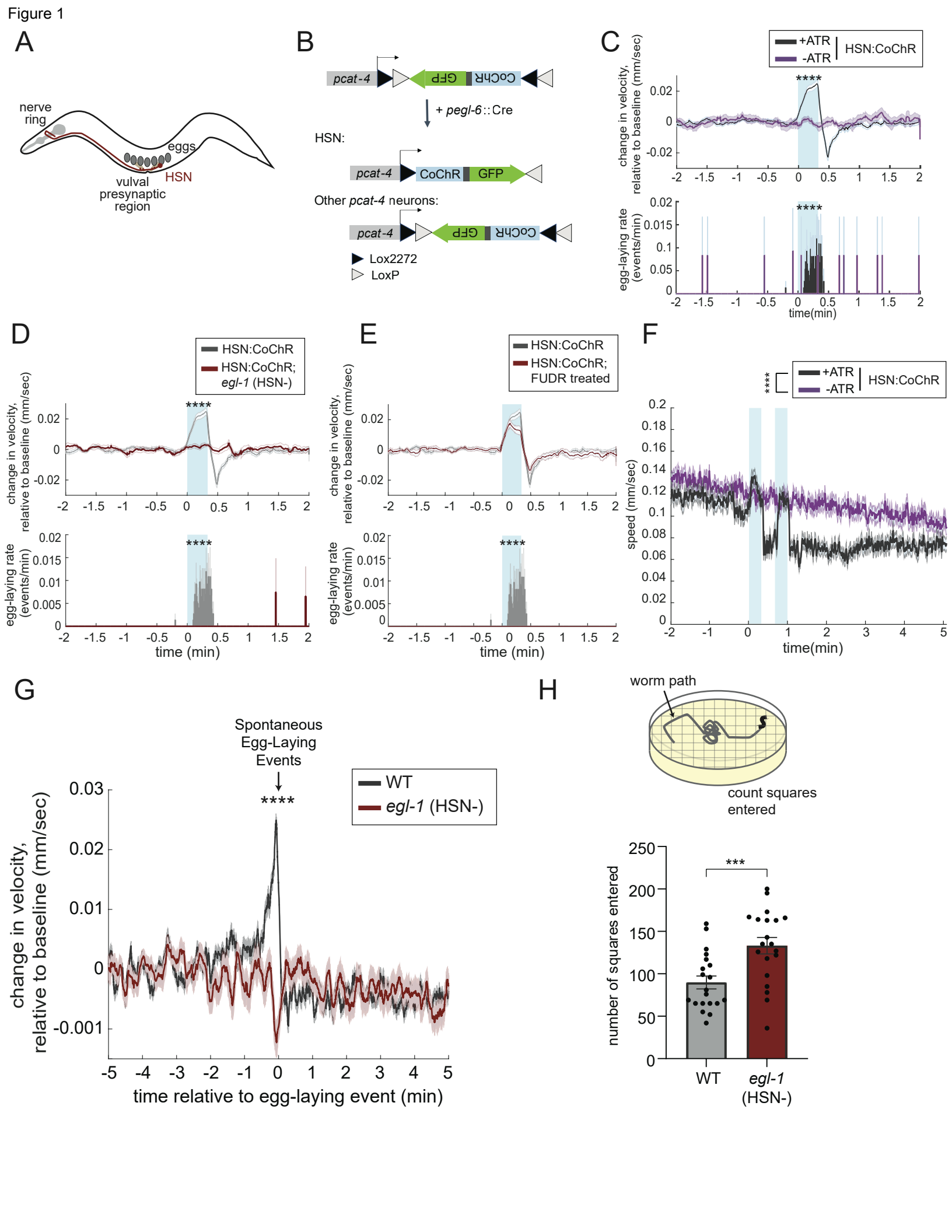
A
nerve ring
eggs
HSN
vulval presynaptic region
B
pcat-4
GFP
CoChR
+ pegl-6::Cre
HSN:
pcat-4
CoChR
GFP
Other pcat-4 neurons:
pcat-4
GFP
CoChR
Lox2272
LoxP
C
+ATR
-ATR
HSN:CoChR
change in velocity, relative to baseline (mm/sec)
egg-laying rate (events/min)
time(min)
D
HSN:CoChR
HSN:CoChR; egl-1 (HSN-)
change in velocity, relative to baseline (mm/sec)
egg-laying rate (events/min)
time (min)
E
HSN:CoChR
HSN:CoChR; FUDR treated
change in velocity, relative to baseline (mm/sec)
egg-laying rate (events/min)
time (min)
F
+ATR
-ATR
HSN:CoChR
speed (mm/sec)
time(min)
G
Spontaneous Egg-Laying Events
WT
egl-1 (HSN-)
change in velocity, relative to baseline (mm/sec)
time relative to egg-laying event (min)
H
worm path
count squares entered
number of squares entered
WT
egl-1 (HSN-)

Figure 2

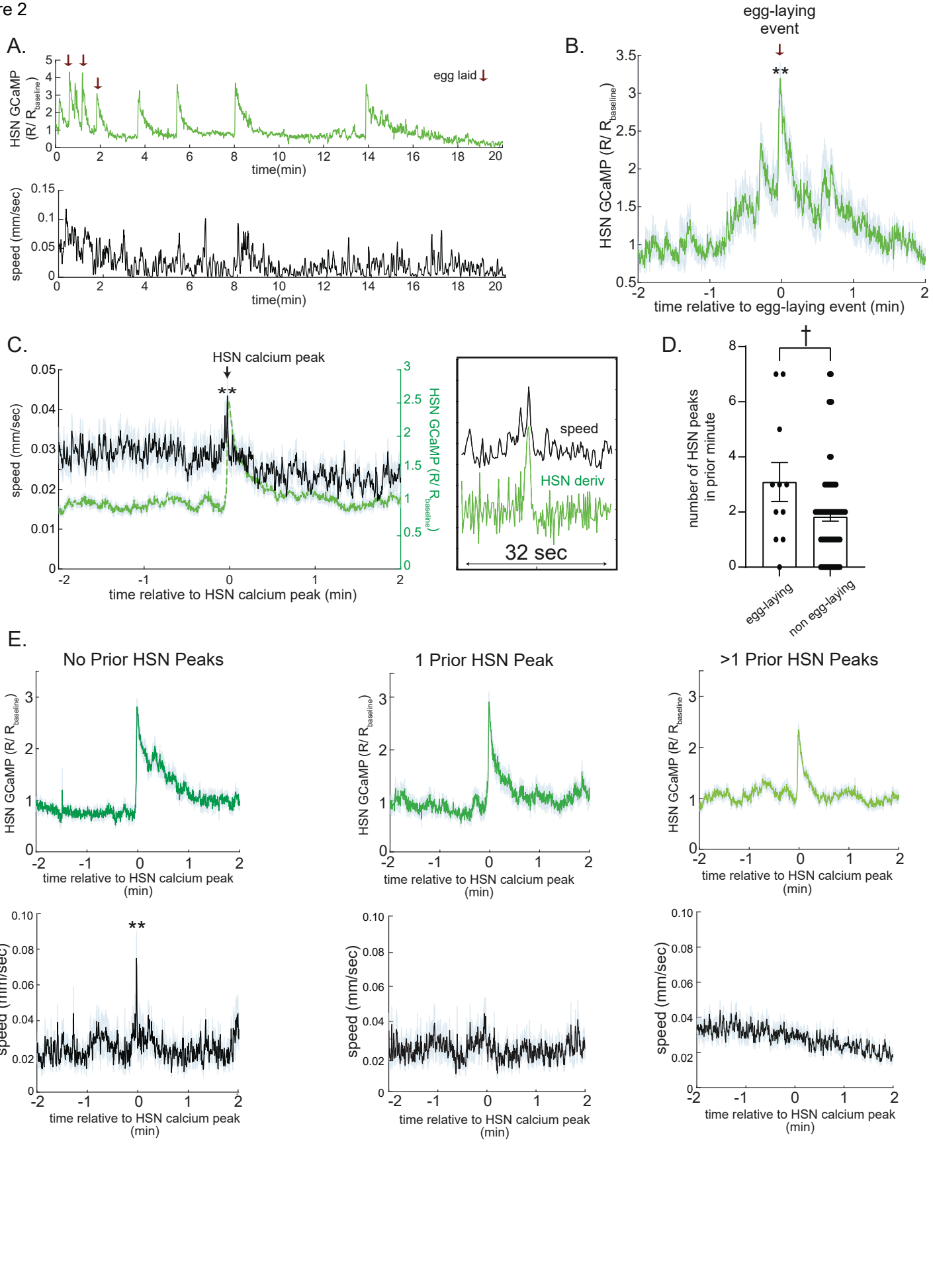
A.
HSN GCaMP (R/ R baseline)
egg laid
time(min)
speed (mm/sec)
time(min)
B.
egg-laying event
**
HSN GCaMP (R/ R baseline)
time relative to egg-laying event (min)
C.
HSN calcium peak
**
speed (mm/sec)
HSN GCaMP (R/ R baseline)
time relative to HSN calcium peak (min)
speed
HSN deriv
32 sec
D.
†
number of HSN peaks in prior minute
egg-laying
non egg-laying
E.
No Prior HSN Peaks
1 Prior HSN Peak
>1 Prior HSN Peaks
HSN GCaMP (R/ R baseline)
time relative to HSN calcium peak (min)
**
speed (mm/sec)
time relative to HSN calcium peak (min)

Figure 3

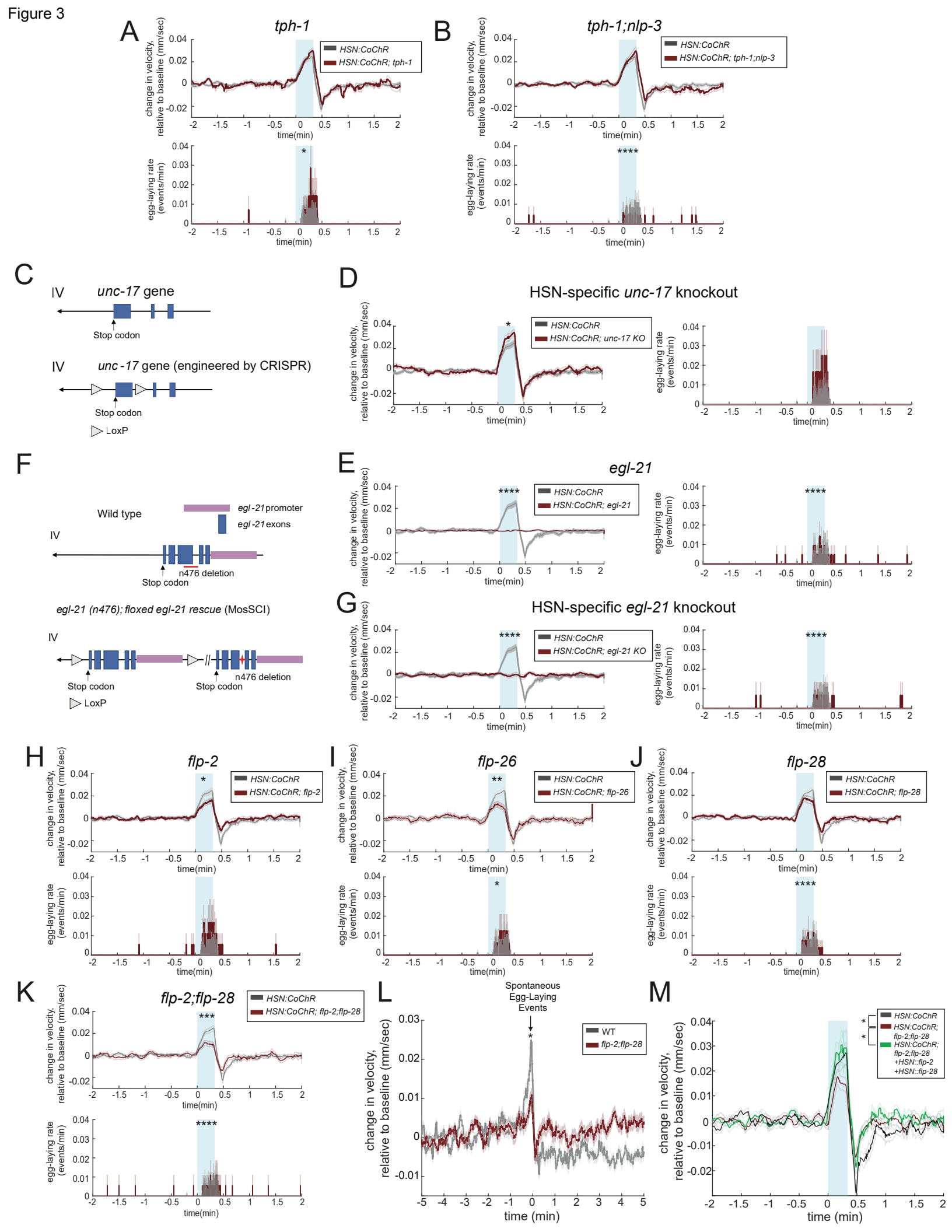
A
tph-1
HSN:CoChR
HSN:CoChR; tph-1
change in velocity, relative to baseline (mm/sec)
egg-laying rate (events/min)
time(min)
*
B
tph-1;nlp-3
HSN:CoChR
HSN:CoChR; tph-1;nlp-3
****
C
IV
unc-17 gene
Stop codon
unc-17 gene (engineered by CRISPR)
LoxP
D
HSN-specific unc-17 knockout
HSN:CoChR
HSN:CoChR; unc-17 KO
E
egl-21
HSN:CoChR
HSN:CoChR; egl-21
F
Wild type
egl-21 promoter
egl-21 exons
n476 deletion
egl-21 (n476); floxed egl-21 rescue (MosSCI)
G
HSN-specific egl-21 knockout
HSN:CoChR
HSN:CoChR; egl-21 KO
H
flp-2
HSN:CoChR
HSN:CoChR; flp-2
I
flp-26
**
HSN:CoChR
HSN:CoChR; flp-26
J
flp-28
HSN:CoChR
HSN:CoChR; flp-28
K
flp-2;flp-28
***
HSN:CoChR
HSN:CoChR; flp-2;flp-28
L
Spontaneous Egg-Laying Events
WT
flp-2;flp-28
time (min)
M
HSN:CoChR
HSN:CoChR; flp-2;flp-28
HSN:CoChR; flp-2;flp-28 +HSN::flp-2 +HSN::flp-28

Figure 4

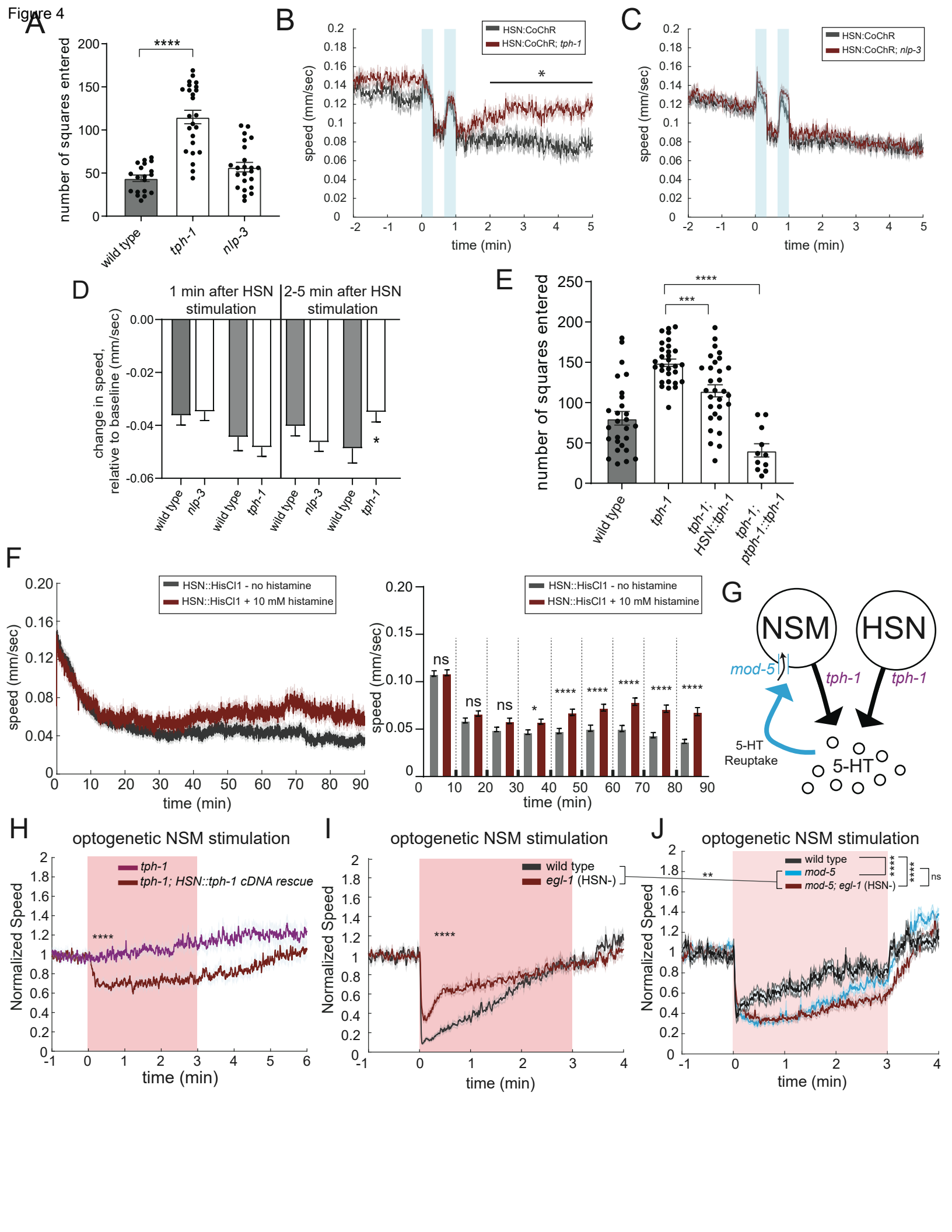
A
number of squares entered
****
wild type
tph-1
nlp-3
B
HSN:CoChR
HSN:CoChR; tph-1
speed (mm/sec)
time (min)
C
HSN:CoChR
HSN:CoChR; nlp-3
speed (mm/sec)
time (min)
D
1 min after HSN stimulation
2-5 min after HSN stimulation
change in speed, relative to baseline (mm/sec)
wild type
nlp-3
tph-1
E
number of squares entered
****
***
wild type
tph-1
tph-1; HSN::tph-1
tph-1; ptph-1::tph-1
F
HSN::HisCl1 - no histamine
HSN::HisCl1 + 10 mM histamine
speed (mm/sec)
time (min)
ns
G
NSM
HSN
mod-5
tph-1
tph-1
5-HT Reuptake
5-HT
H
optogenetic NSM stimulation
tph-1
tph-1; HSN::tph-1 cDNA rescue
Normalized Speed
time (min)
I
optogenetic NSM stimulation
wild type
egl-1 (HSN-)
Normalized Speed
time (min)
J
optogenetic NSM stimulation
wild type
mod-5
mod-5; egl-1 (HSN-)
ns
Normalized Speed
time (min)

Figure 5

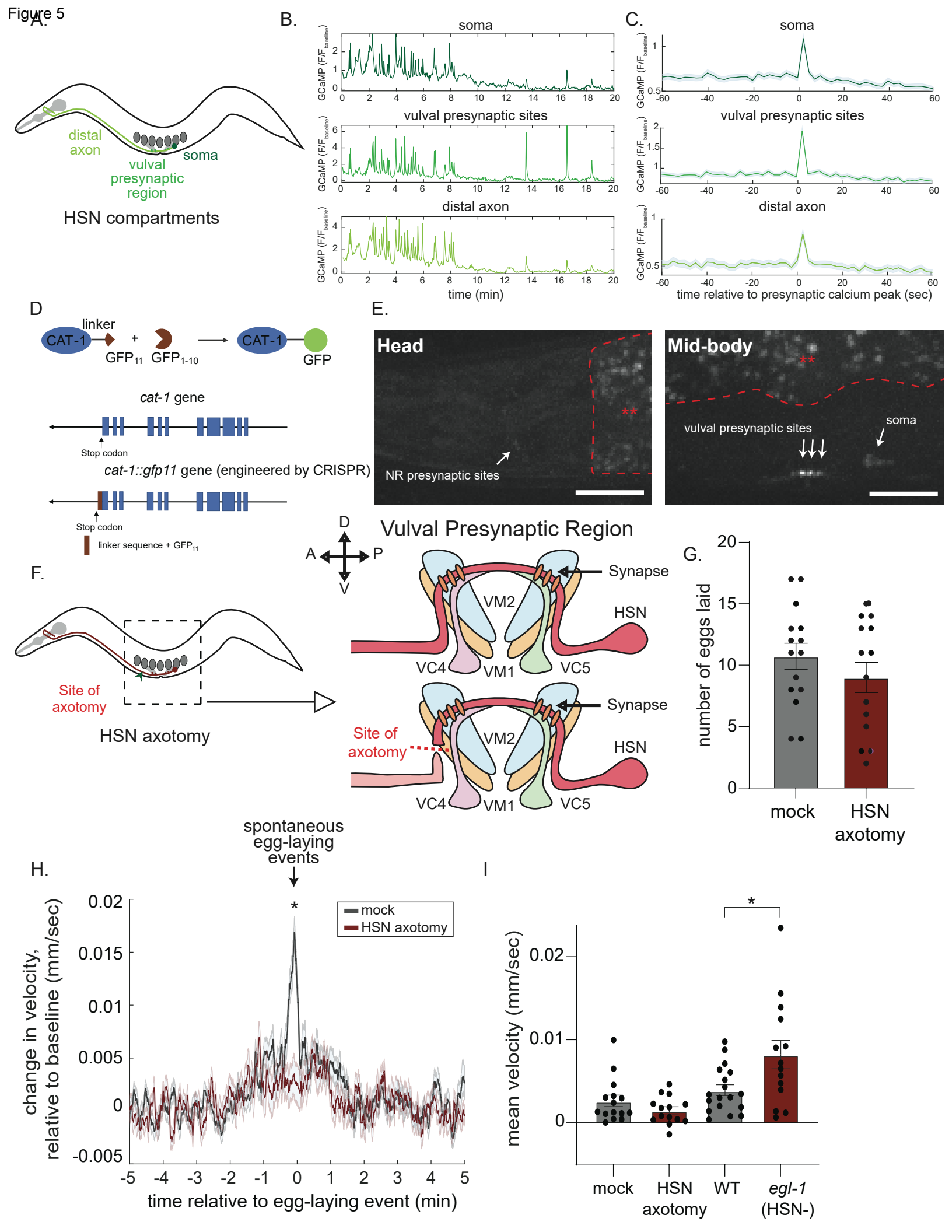
A.
distal axon
soma
vulval presynaptic region
HSN compartments
B.
soma
vulval presynaptic sites
distal axon
GCaMP (F/F baseline)
time (min)
C.
soma
vulval presynaptic sites
distal axon
GCaMP (F/F baseline)
time relative to presynaptic calcium peak (sec)
D
linker
CAT-1
GFP11
GFP1-10
GFP
cat-1 gene
Stop codon
cat-1::gfp11 gene (engineered by CRISPR)
Stop codon
linker sequence + GFP11
E.
Head
NR presynaptic sites
Mid-body
vulval presynaptic sites
soma
F.
Site of axotomy
HSN axotomy
Vulval Presynaptic Region
D
A
P
V
Synapse
HSN
VM2
VC4
VM1
VC5
Site of axotomy
G.
number of eggs laid
mock
HSN axotomy
spontaneous egg-laying events
H.
change in velocity, relative to baseline (mm/sec)
mock
HSN axotomy
time relative to egg-laying event (min)
I
mean velocity (mm/sec)
mock
HSN axotomy
WT
egl-1 (HSN-)

Figure 6

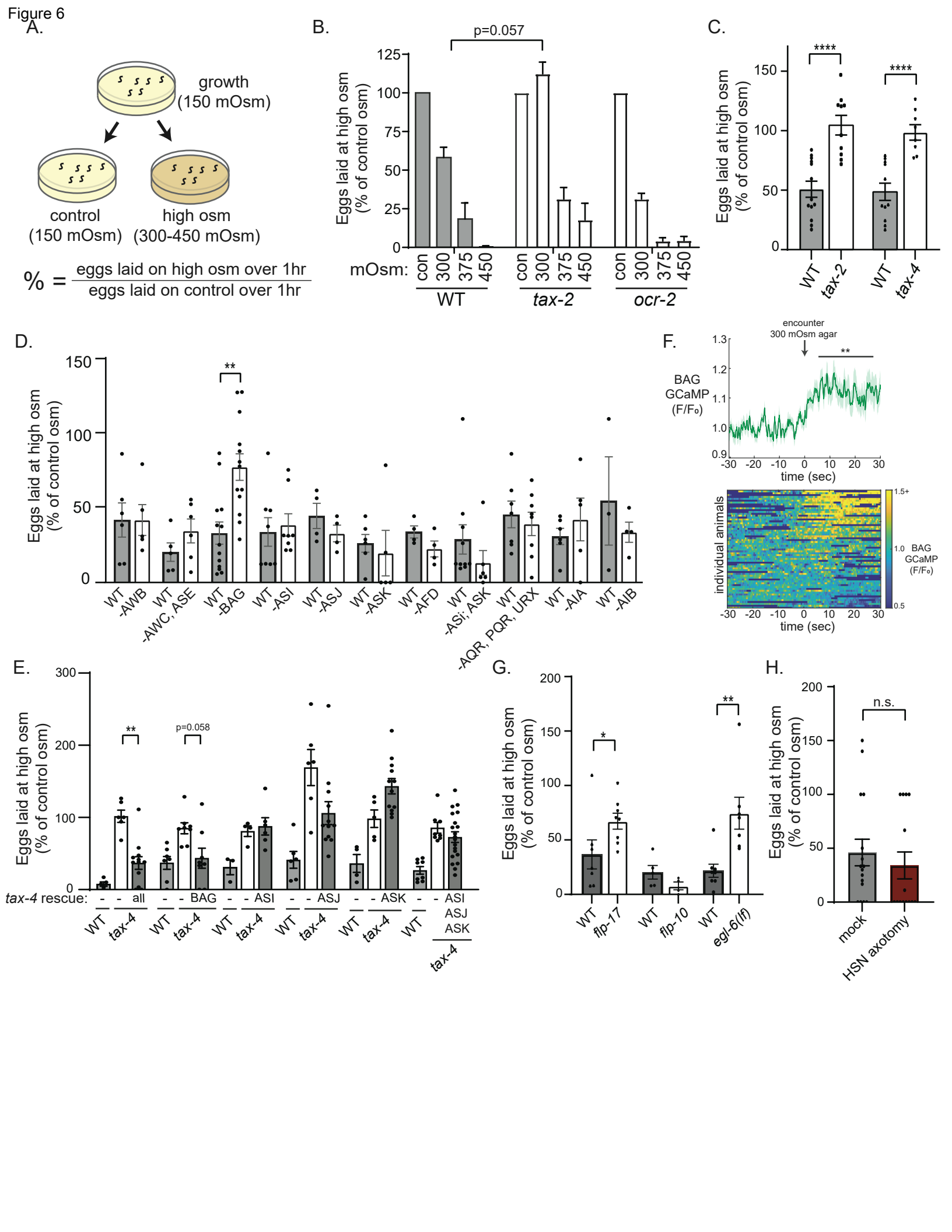
A.
growth
(150 mOsm)
control
(150 mOsm)
high osm
(300-450 mOsm)
% = eggs laid on high osm over 1hr / eggs laid on control over 1hr
B.
p=0.057
Eggs laid at high osm
(% of control osm)
mOsm: con 300 375 450
WT
tax-2
ocr-2
C.
****
****
WT
tax-2
WT
tax-4
D.
**
-AWB
-AWC, ASE
-BAG
-ASI
-ASJ
-ASK
-AFD
-ASi; ASK
-AQR, PQR, URX
-AIA
-AIB
F.
encounter
300 mOsm agar
BAG
GCaMP
(F/F0)
time (sec)
individual animals
E.
**
p=0.058
tax-4 rescue:
all
BAG
ASI
ASJ
ASK
ASI
ASJ
ASK
tax-4
G.
*
**
flp-17
flp-10
egl-6(lf)
H.
n.s.
mock
HSN axotomy

A

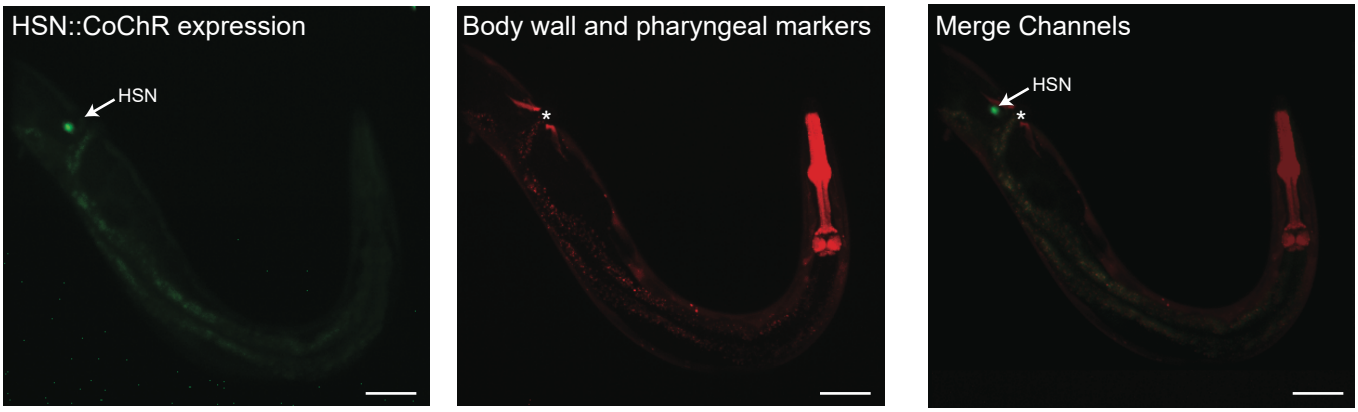
HSN::CoChR expression
HSN
Body wall and pharyngeal markers
*
Merge Channels
HSN
*

B

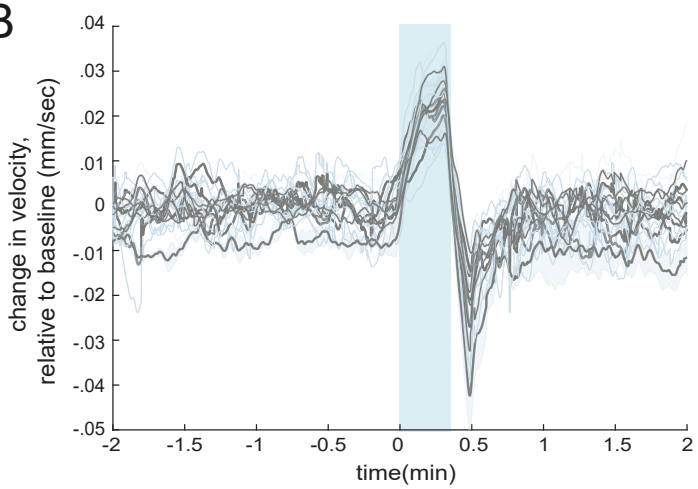
change in velocity, relative to baseline (mm/sec)
.04
.03
.02
.01
0
-.01
-.02
-.03
-.04
-.05
-2
-1.5
-1
-0.5
0
0.5
1
1.5
2
time(min)

C

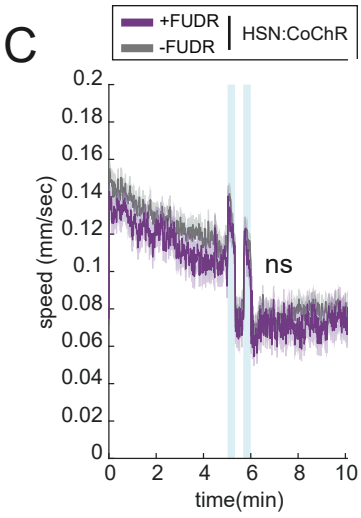
+FUDR
-FUDR
HSN:CoChR
speed (mm/sec)
0.2
0.18
0.16
0.14
0.12
0.1
0.08
0.06
0.04
0.02
0
ns
0
2
4
6
8
10
time(min)

Supplemental Figure 1. HSN::CoChR expression and activation, related to Figure 1.

(A) Representative images of HSN::CoChR-sl2-GFP expression (left), along with body wall and pharyngeal markers (middle), and a composite image (right). Arrows indicate HSN soma. Asterisks indicate vulva position. Scale bar, 50 um.

(B) Average wild-type HSN::CoChR effects on velocity, shown for different recording days. Each line represents the average change in velocity elicited by HSN::CoChR stimulation across wild-type animals recorded on a given day. A one-factor ANOVA on the velocity change (where the factor was recording date) did not reveal any significant effect of recording date ($F=1.162$, $p=0.3738$).

(C) Animal speed during several bouts of HSN::CoChR stimulation for animals recently transferred to food plates. Data are shown for HSN::CoChR animals either treated with FUDR or not. Data are displayed as in Fig. 1F and statistics were performed as in Fig 1F. n = 69 animals for the FUDR-treated group, and 195 animals for the no-FUDR control.

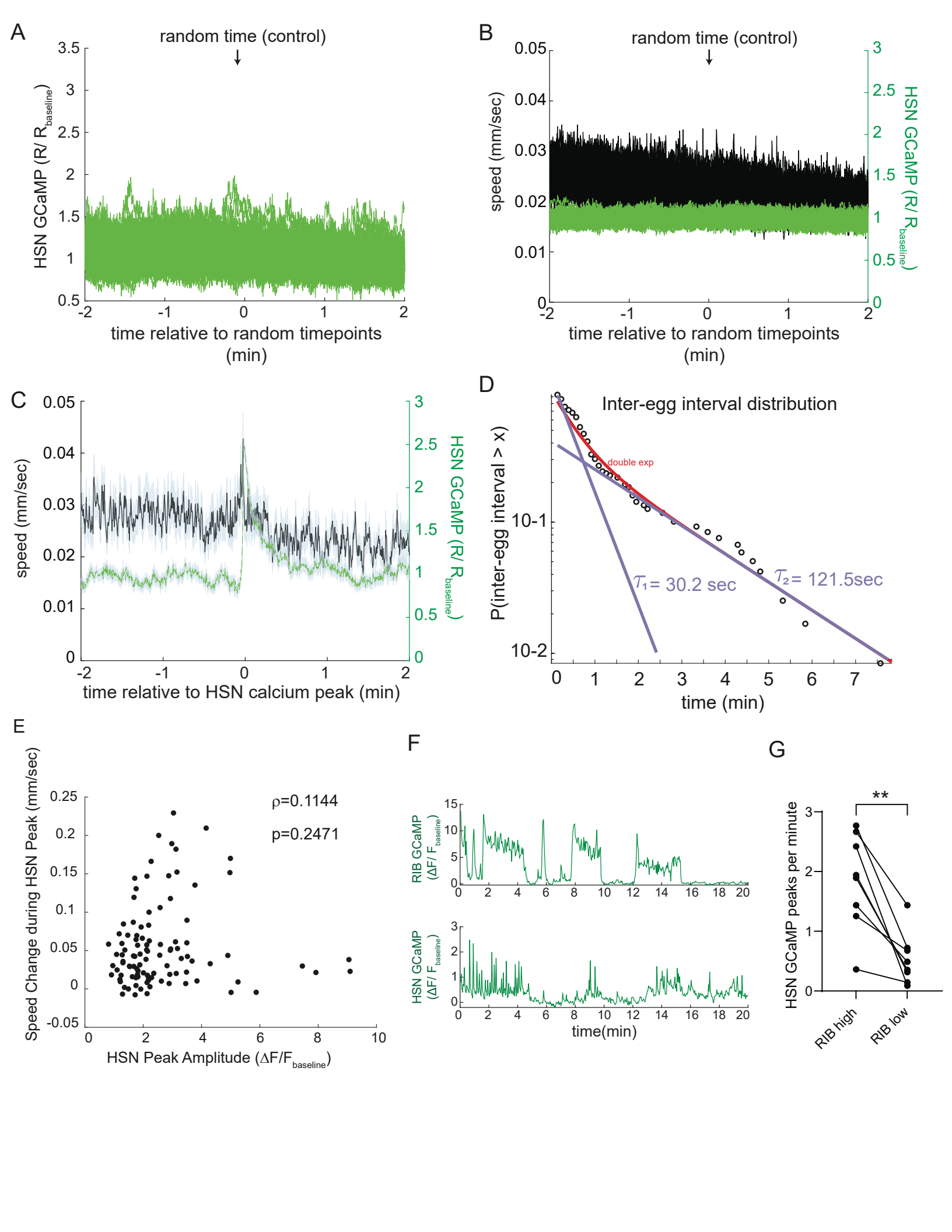
A
random time (control)
HSN GCaMP (R/ R baseline)
time relative to random timepoints (min)
B
random time (control)
speed (mm/sec)
HSN GCaMP (R/ R baseline)
time relative to random timepoints (min)
C
speed (mm/sec)
HSN GCaMP (R/ R baseline)
time relative to HSN calcium peak (min)
D
Inter-egg interval distribution
P(inter-egg interval > x)
double exp
τ1= 30.2 sec
τ2= 121.5sec
time (min)
E
Speed Change during HSN Peak (mm/sec)
ρ=0.1144
p=0.2471
HSN Peak Amplitude (ΔF/F baseline)
F
RIB GCaMP (ΔF/ F baseline)
HSN GCaMP (ΔF/ F baseline)
time(min)
G
HSN GCaMP peaks per minute
**
RIB high
RIB low

Supplemental Figure 2. HSN GCaMP analyses, and the correlation between HSN and RIB activity, related to Figure 2.

(A) Event-triggered averages showing average HSN GCaMP signal surrounding randomly chosen timepoints, as a control for Fig. 2B. Each line is the mean of 16 timepoints (matching the n in Fig. 2B), and this control was run 100 times, resulting in 100 lines.

(B) Event-triggered averages showing average speed (black) and HSN GCaMP (green) surrounding randomly chosen timepoints, as a control for Fig. 2C. Each line is the mean of 104 timepoints (matching the n in Fig. 2C), and this control was run 100 times, resulting in 100 lines.

(C) Event-triggered average showing average animal speed surrounding HSN calcium peaks. This plot only includes HSN calcium peaks that were not accompanied by egg-laying. Note that speeding still occurs during these peaks.

(D) Complementary cumulative distribution function (ccdf) showing distribution of intervals between HSN calcium peaks. This distribution was best fit by a double exponential (red). The slopes of each exponential are shown in blue and the tau values are also displayed. The shorter distribution is characterized by a tau of ~30s, whereas the longer distribution is characterized by a tau of ~2min.

(E) Scatterplot showing the per-peak relationship between HSN calcium peak amplitude and speeding amplitude during that HSN peak. n = 104 peaks across 15 animals. There is no significant relationship (see inset correlation coefficient and p-values).

(F) Example calcium traces of RIB and HSN from a joint calcium recording of both neurons in immobilized animals.

(G) Frequency of HSN calcium peaks that occurred while RIB was high (i.e. network was in a 'forward' state) or low (i.e. network was in a 'reverse' state). Dots are individual animals. Connected dots represent the same animals. n = 8 animals. **$p<0.01$, Wilcoxon signed rank test.

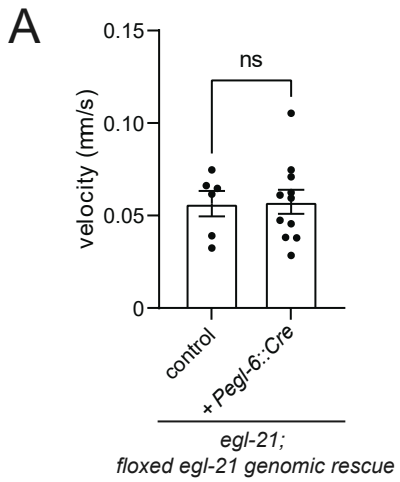
A
0.15
0.10
0.05
0
velocity (mm/s)
ns
control
+Pegl-6::Cre
egl-21;
floxed egl-21 genomic rescue

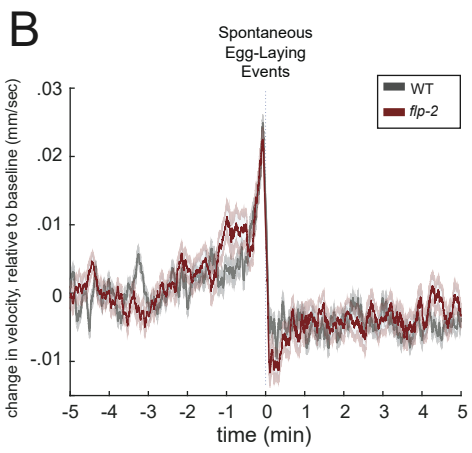
B
Spontaneous
Egg-Laying
Events
WT
flp-2
change in velocity, relative to baseline (mm/sec)
.03
.02
.01
0
-.01
-5 -4 -3 -2 -1 0 1 2 3 4 5
time (min)

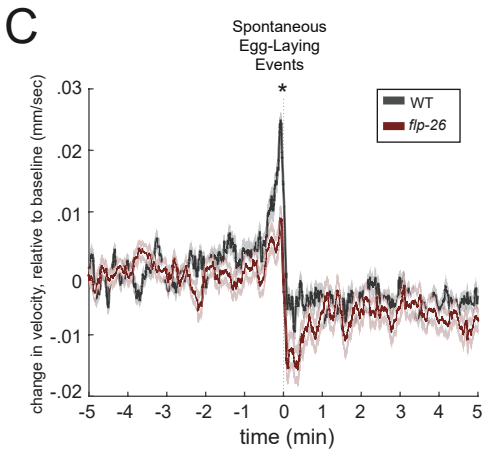
C
Spontaneous
Egg-Laying
Events
*
WT
flp-26
change in velocity, relative to baseline (mm/sec)
.03
.02
.01
0
-.01
-.02
-5 -4 -3 -2 -1 0 1 2 3 4 5
time (min)

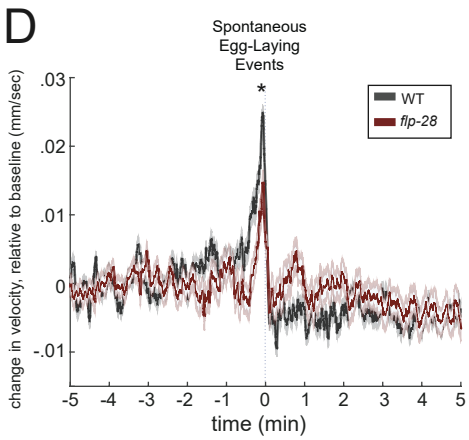
D
Spontaneous
Egg-Laying
Events
*
WT
flp-28
change in velocity, relative to baseline (mm/sec)
.03
.02
.01
0
-.01
-5 -4 -3 -2 -1 0 1 2 3 4 5
time (min)

Supplemental Figure 3. Baseline locomotion of *egl-21; floxed egl-21 genomic rescue* animals and native egg-laying events in peptide mutants, related to Figure 3.

(A) Baseline mean velocity of *egl-21; floxed egl-21 genomic rescue* animals without (control) or with *pegl-6::Cre* expression in the absence of food. Dots show individual animals; bars are means and error bars are SEM. n = 6 animals for control and 11 animals for *pegl-6::Cre* expressing animals.

(B) Event-triggered averages for time periods surrounding native egg-laying events in *flp-2(gk1039)* animals. Data are shown as in Fig. 1G and statistics were performed as in Fig. 1G. n = 21 animals for wild-type (518 egg events) (same data as Fig. 1G) and n = 6 animals for *flp-2* (194 egg-laying events).

(C) Event-triggered averages for time periods surrounding native egg-laying events in *flp-26(gk3015)* animals. Data are shown as in Fig. 1G and statistics were performed as in Fig. 1G. n = 21 animals for wild-type (518 egg events) (same data as Fig. 1G) and n = 6 animals for *flp-26* (162 egg-laying events). *p<0.05, Mann-Whitney U test, Bonferroni-corrected for *flp-2*, *flp-26* and *flp-28* single mutants.

(D) Event-triggered averages for time periods surrounding native egg-laying events in *flp-28(flv11)* animals. Data are shown as in Fig. 1G and statistics were performed as in Fig. 1G. n = 21 animals for wild-type (518 egg events) (same data as Fig. 1G) and n = 6 animals (159 egg-laying events) for *flp-28*. *p<0.05, Mann-Whitney U test, Bonferroni-corrected for *flp-2*, *flp-26* and *flp-28* single mutants.

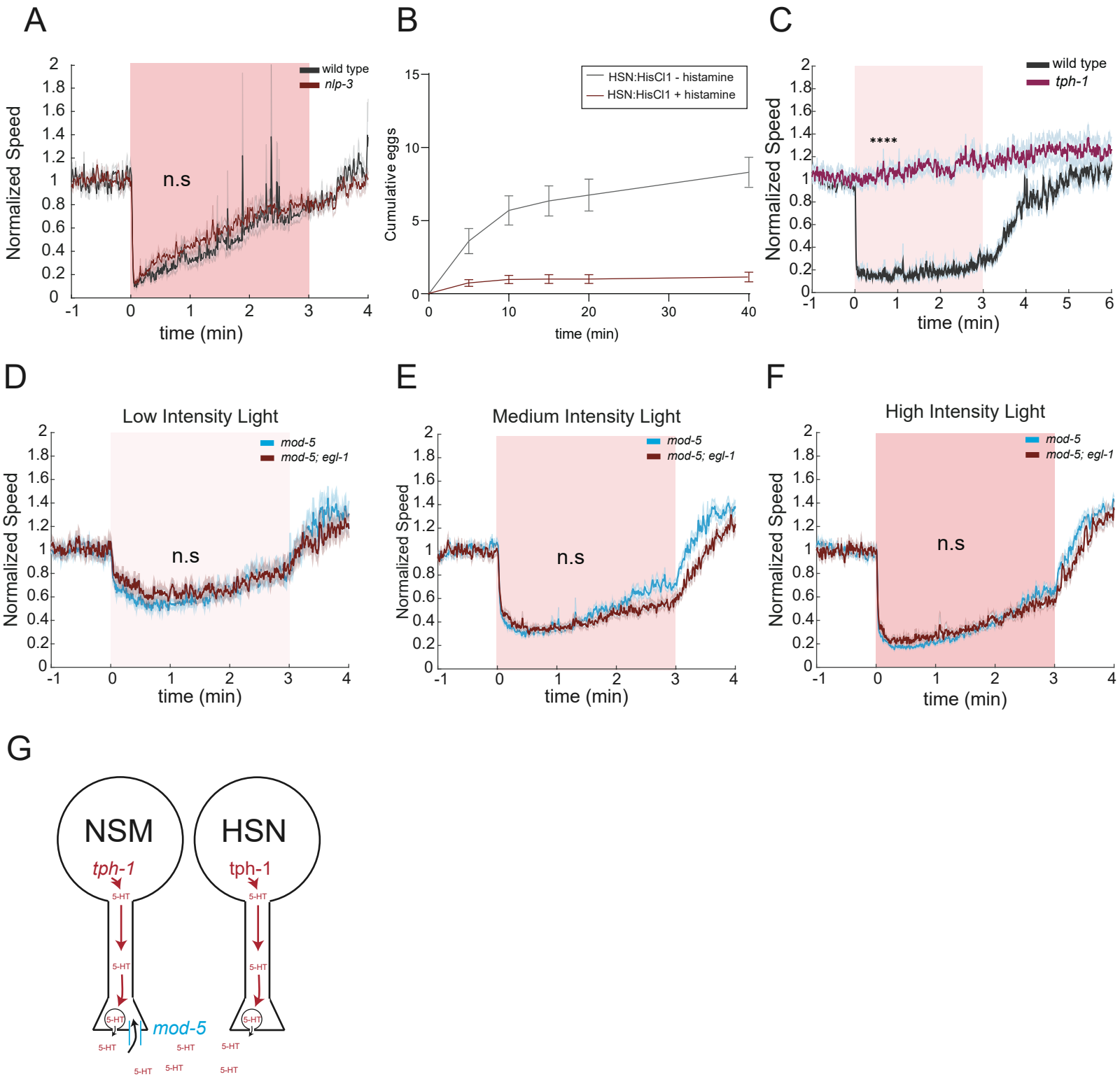
A
Normalized Speed
wild type
nlp-3
n.s
time (min)
B
Cumulative eggs
HSN:HisCl1 - histamine
HSN:HisCl1 + histamine
time (min)
C
Normalized Speed
wild type
tph-1
****
time (min)
D
Low Intensity Light
Normalized Speed
mod-5
mod-5; egl-1
n.s
time (min)
E
Medium Intensity Light
Normalized Speed
mod-5
mod-5; egl-1
n.s
time (min)
F
High Intensity Light
Normalized Speed
mod-5
mod-5; egl-1
n.s
time (min)
G
NSM
HSN
tph-1
tph-1
5-HT
mod-5

Supplemental Figure 4. Egg-laying of HSN::HisCl animals and NSM::Chrimson responses, related to Figure 4.

(A) Event-triggered averages depicting the average change in animal speed upon NSM::Chrimson stimulation with red light illumination in wild-type and *nlp-3(n4897)* animals. Lines show means; and error shading shows SEM. n = 59 for wild-type animals and 73 for *nlp-3(n4897)* animals.

(B) Egg-laying of HSN::HisCl animals either exposed to histamine or not. Animals for this experiment were transferred to +his or -his plates immediately before this assay (i.e. at t = 0 min), and eggs laid were counted at different time points, up to 40min after transfer. Note that egg-laying is reduced even at the first time point, indicating the HSN::HisCl inhibits egg-laying within minutes of first exposure to histamine. n = 35 plates for HSN::HisCl with histamine and 20 plates for no histamine control group, with 3 animals on each plate.

(C) Event-triggered averages depicting the average change in animal speed upon NSM::Chrimson stimulation with red light illumination in wild-type and *tph-1(mg280)* animals. Animals were starved for 3 hours before the assays. Lines show means; and error shading shows SEM. n = 77-390 animals. ***p<0.0001, unpaired t-test.

(D to F) Event-triggered averages depicting the average change in animal speed upon NSM::Chrimson stimulation with different light intensities in *mod-5(n822)* and *mod-5(n822);egl-1(n487gf)* animals, with panel C being the lowest intensity and panel E the highest. n = 51-248 animals.

(G) Cartoon illustrating serotonin release and re-uptake by NSM and HSN neurons.

A.

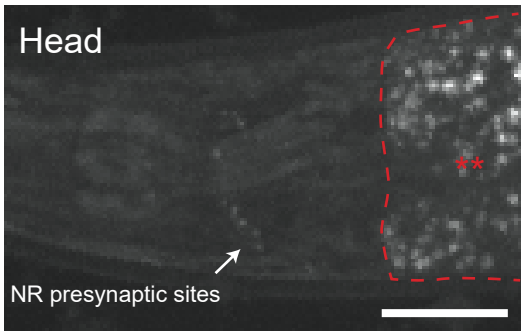
Head
NR presynaptic sites

B.

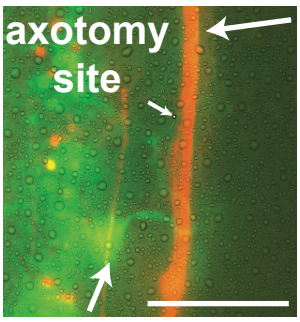
axotomy site
ventral cord (pan-neural mScarlett)
HSN

C.

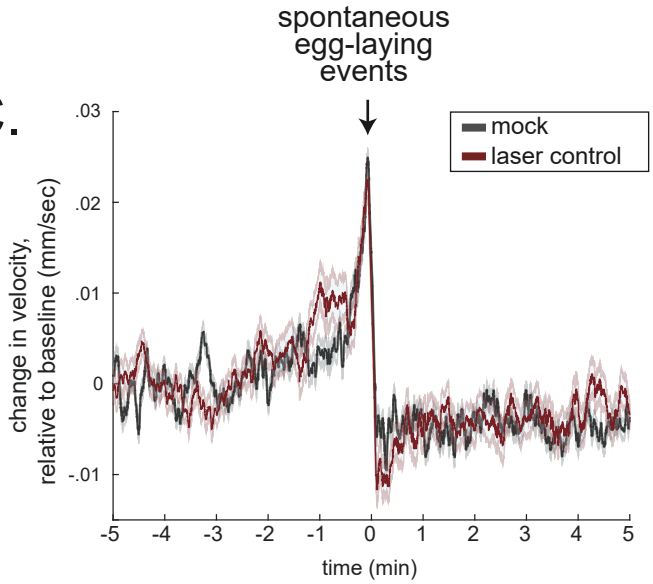
spontaneous egg-laying events
mock
laser control
change in velocity, relative to baseline (mm/sec)
.03
.02
.01
0
-.01
-5
-4
-3
-2
-1
0
1
2
3
4
5
time (min)

Supplemental Figure 5. Representative image of HSN axotomy and native egg-laying events of the laser control group, related to Figure 5.

(A) Longer exposure image of HSN CAT-1::GFP puncta in the head region, of the same animal displayed in Fig. 5E. These puncta are very faint relative to the CAT-1::GFP puncta that HSN displays in the vulval presynaptic region. Scale bar, 25 um.

(B) Fluorescent image of the vulval region of an example animal from the transgenic line that was used for laser axotomy. This strain has HSN::GFP and pan-neural::mScarlett, as indicated. The image is being used to illustrate the site of HSN laser axotomy (note the small dot at the tip of the white arrow for axotomy site, which is the exact cut site). Scale bar, 20 um

(C) Event-triggered average showing average animal velocity surrounding native, spontaneous egg-laying events. Data are shown for mock and laser control animals, in which a laser was fired adjacent to the HSN axon, at the same settings used for the actual axotomy in Fig. 5H. Data are shown as in Fig. 1G and statistics were designed in the same manner as in Fig. 1G. Lines show means and error shading shows SEM. n = 17 animals for mock (118 egg events); n = 17 animals for laser control (108 egg events). Note that the mock group was specifically paired to these laser controls (i.e. run side-by-side in same experiment) and are different animals from the mock animals in the actual axotomy (Fig. 5H).

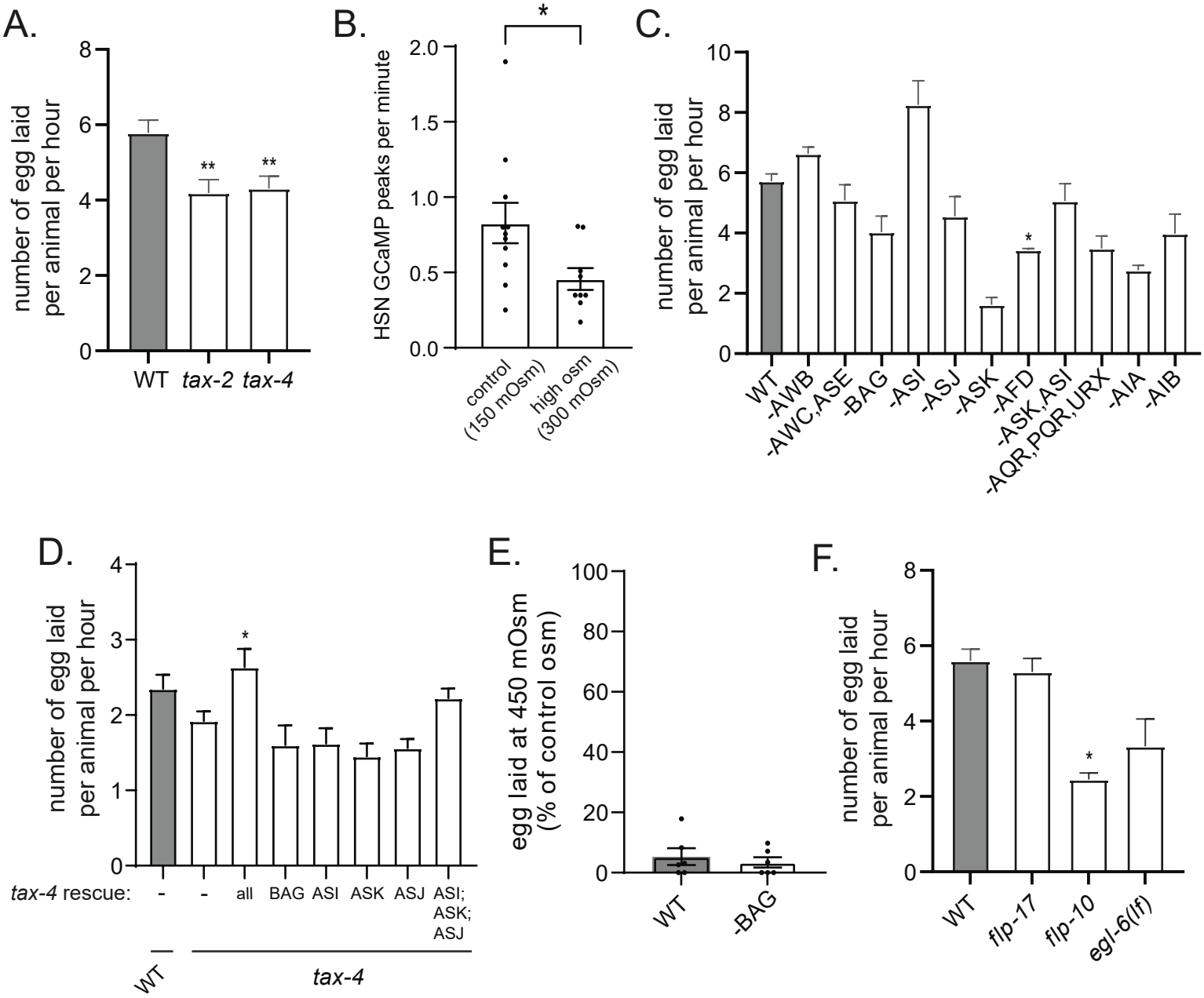
A.
number of egg laid per animal per hour
WT
tax-2
tax-4
B.
HSN GCaMP peaks per minute
control (150 mOsm)
high osm (300 mOsm)
C.
number of egg laid per animal per hour
WT
-AWB
-AWC,ASE
-BAG
-ASI
-ASJ
-ASK
-AFD
-ASK,ASI
-AQR,PQR,URX
-AIA
-AIB
D.
number of egg laid per animal per hour
tax-4 rescue:
all
BAG
ASI
ASK
ASJ
ASI; ASK; ASJ
WT
tax-4
E.
egg laid at 450 mOsm (% of control osm)
WT
-BAG
F.
number of egg laid per animal per hour
WT
flp-17
flp-10
egl-6(lf)

Supplemental Figure 6. HSN activity in high osmolarity and baseline egg-laying rates for indicated genotypes, related to Figure 6.

(A) Baseline egg-laying rates on normal osmolarity (150 mOsm) plates for the indicated genotypes that are also displayed in Fig. 6C. Note that these are the raw values for control data displayed in Fig. 6C. **$p<0.01$, Mann-Whitney tests comparing day-matched groups. (WT data are shown aggregated across all relevant days for simplicity, but statistics were performed comparing animals to their day-matched wild-type animals)

(B) Frequency of HSN GCaMP peaks in freely-moving animals exploring agar pads with either 150 mOsm environment or 300 mOsm environment (via sorbitol addition). n = 9-11 animals. *$p<0.05$, unpaired t-test.

(C) Baseline egg-laying rates on normal osmolarity (150 mOsm) plates for the indicated genotypes that are also displayed in Fig. 6D. Note that these are the raw values for control data displayed in Fig. 6D. For display purpose, data points of wild-type animals were pooled together. Statistics were done by only comparing day-matched groups. *$p<0.05$, Bonferroni corrected Mann-Whitney tests comparing day-matched groups. (WT data are shown aggregated across all relevant days for simplicity, but statistics were performed comparing animals to their day-matched wild-type animals)

(D) Baseline egg-laying rates on normal osmolarity (150 mOsm) plates for the indicated genotypes that are also displayed in Fig. 6E. Note that these are the raw values for control data displayed in Fig. 6E. *$p<0.05$, Bonferroni corrected Mann-Whitney tests comparing the indicated day-matched groups. (WT data are shown aggregated across all relevant days for simplicity, but statistics were performed comparing animals to their day-matched wild-type animals)

(E) Egg-laying inhibition induced by exposure to 450 mOsm agar, compared to standard 150 mOsm conditions, shown for wild-type animals and BAG-ablated animals. n = 6 plates (with 10 animals each) per condition.

(F) Baseline egg-laying rates on normal osmolarity (150 mOsm) plates for the indicated genotypes that are also displayed in Fig. 6G. Note that these are the raw values for control data displayed in Fig. 6G. *$p<0.05$, Mann-Whitney tests comparing the indicated day-matched groups. (WT data are shown aggregated across all relevant days for simplicity, but statistics were performed by comparing animals to their day-matched wild-type animals)

CELL PRESS DECLARATION OF INTERESTS POLICY

Transparency is essential for a reader's trust in the scientific process and for the credibility of published articles. At Cell Press, we feel that disclosure of competing interests is a critical aspect of transparency. Therefore, we require a "declaration of interests" section in which all authors disclose any financial or other interests related to the submitted work that (1) could affect or have the perception of affecting the author's objectivity or (2) could influence or have the perception of influencing the content of the article.

What types of articles does this apply to?

We require that you disclose competing interests for all submitted content by completing and submitting the form below. We also require that you include a "declaration of interests" section in the text of all articles even if there are no interests to declare.

What should I disclose?

We require that you and all authors disclose any personal financial interests (e.g., stocks or shares in companies with interests related to the submitted work or consulting fees from companies that could have interests related to the work), professional affiliations, advisory positions, board memberships (including membership on a journal's advisory board when publishing in that journal), or patent holdings that are related to the subject matter of the contribution. As a guideline, you need to declare an interest for (1) any affiliation associated with a payment or financial benefit exceeding $10,000 p.a. or 5% ownership of a company or (2) research funding by a company with related interests. You do not need to disclose diversified mutual funds, 401ks, or investment trusts.

Authors should also disclose relevant financial interests of immediate family members. Cell Press uses the Public Health Service definition of "immediate family member," which includes spouse and dependent children.

Where do I declare competing interests?

Competing interests should be disclosed on this form as well as in a "declaration of interests" section in the manuscript. This section should include financial or other competing interests as well as affiliations that are not included in the author list. Examples of "declaration of interests" language include:

> "AUTHOR is an employee and shareholder of COMPANY."
> "AUTHOR is a founder of COMPANY and a member of its scientific advisory board."

NOTE: Primary affiliations should be included with the author list and do not need to be included in the "declaration of interests" section. Funding sources should be included in the "acknowledgments" section and also do not need to be included in the "declaration of interests" section. (A small number of front-matter article types do not include an "acknowledgments" section. For these articles, reporting of funding sources is not required.)

What if there are no competing interests to declare?

If you have no competing interests to declare, please note that in the "declaration of interests" section with the following wording:

> "The authors declare no competing interests."

August 1, 2023

CELL PRESS DECLARATION OF INTERESTS FORM

If submitting materials via Editorial Manager, please complete this form and upload with your initial submission. Otherwise, please email as an attachment to the editor handling your manuscript.

Please complete each section of the form and insert any necessary "declaration of interests" statement in the text box at the end of the form. A matching statement should be included in a "declaration of interests" section in the manuscript.

Institutional affiliations

We require that you list the current institutional affiliations of all authors, including academic, corporate, and industrial, on the title page of the manuscript. ***Please select one of the following:***

☒ All affiliations are listed on the title page of the manuscript.

☐ I or other authors have additional affiliations that we have noted in the "declaration of interests" section of the manuscript and on this form below.

Funding sources

We require that you disclose all funding sources for the research described in this work. ***Please confirm the following:***

☒ All funding sources for this study are listed in the "acknowledgments" section of the manuscript.*

*A small number of front-matter article types do not include an "acknowledgments" section. For these, reporting funding sources is not required.

Competing financial interests

We require that authors disclose any financial interests and any such interests of immediate family members, including financial holdings, professional affiliations, advisory positions, board memberships, receipt of consulting fees, etc., that:

(1) could affect or have the perception of affecting the author's objectivity, *or*
(2) could influence or have the perception of influencing the content of the article.

Please select one of the following:

☒ We, the authors and our immediate family members, have no financial interests to declare.

☐ We, the authors, have noted any financial interests in the "declaration of interests" section of the manuscript and on this form below, and we have noted interests of our immediate family members.

Advisory/management and consulting positions

We require that authors disclose any position, be it a member of a board or advisory committee or a paid consultant, that they have been involved with that is related to this study. We also require that members of our journal advisory boards disclose their position when publishing in that journal. ***Please select one of the following:***

☒ We, the authors and our immediate family members, have no positions to declare and are not members of the journal's advisory board.

☐ The authors and/or their immediate family members have management/advisory or consulting relationships noted in the "declaration of interests" section of the manuscript and on this form below.

Patents

We require that you disclose any patents related to this work by any of the authors or their institutions. ***Please select one of the following:***

☒ We, the authors and our immediate family members, have no related patents to declare.

☐ We, the authors, have a patent related to this work, which is noted in the "declaration of interests" section of the manuscript and on this form below, and we have noted the patents of immediate family members.

Please insert any "declaration of interests" statements in this space. This exact text should also be included in the "declaration of interests" section of the manuscript. If no authors have a competing interest, please insert the text, "The authors declare no competing interests."

The authors declare no competing interests.

☒ **On behalf of all authors, I declare that I have disclosed all competing interests related to this work. If any exist, they have been included in the "declaration of interests" section of the manuscript.**